Chapter 12

Photophysics and Quantum Emission Behaviors of Covalently Introduced Defects in Single-Wall Carbon Nanotubes

Stephen K. Doorn*, Han Htoon and Sergei Tretiak

Center for Integrated Nanotechnologies, Los Alamos National Laboratory, Los Alamos, NM, USA

**skdoorn@lanl.gov*

Low-level covalent functionalization of single-wall carbon nanotubes introduces structural defects that are accompanied by new photoluminescent electronic states. Localization of excitons at the defect sites gives rise to a wide range of associated new photophysical phenomena and optical functionality to probe, understand, and harness. Here, we review recent progress in chemistry, electronic structure, spectroscopy, and quantum light emission properties of these intriguing defects and provide some perspective on potential future areas for research in this rapidly developing area of nanotube studies. Current approaches to chemical introduction of photoluminescent defects and synthetic modification of molecular dopants for tuning of emission properties are described. Spectroscopic probes paired with quantum chemistry modeling of the defect states are outlined as an efficient route toward understanding the defect electronic structure. Exciton localization at defects and its consequences for photoluminescence response are also discussed. Such spatial localization of the electronic wavefunction is especially important for introducing new functionality, including expanded possibilities for imaging and sensing applications. We focus on localization as a route for achieving room-temperature single photon emission, important for optical-based quantum information processing. Conditions required for quantum light emission, its demonstration at room temperature, and tunability to telecom wavelengths are shown. We conclude with a discussion of some critical challenges that remain for

understanding and controlling covalent defects in nanotube materials in the areas of chemistry, photophysics, quantum optics, and electro-optic device integration.

Contents

It is difficult to imagine anyone working on carbon nanotubes (CNTs) who has not been influenced or inspired by Millie Dresselhaus. While our most direct interactions with Millie were typically through her exceptional leadership and

contributions to Raman spectroscopy of CNTs, she also made many important contributions related to their photoluminescence (PL). These two important optical responses are linked through the nanotube exciton resonances. This brings to mind the first WONTON meeting in 2005, in which Millie kicked off our discussions by asking two questions that can be paraphrased as: Do excitons exist in nanotubes? Do we need excitons? The answer to both of course is yes. Excitons, or bound states of electron–hole pairs, are the fundamental basis for the rich array of optical behaviors found in CNTs. Our ongoing challenge, however, remains to productively harness these behaviors. A key development towards this end is the covalent introduction of defects, which introduce new photophysical response to explore. Through the associated exciton localization, PL is enhanced and new functionality emerges, with great promise for advancing photonic applications of these materials.

1. Introduction

Single-wall carbon nanotubes (SWCNTs) embody unique structural characteristics,[1] can serve as semiconducting or metallic elements in nanoscale electronics,[2] and act as near-infrared light emitters.[3] As multifunctional nanomaterials, they thus hold significant applications potential. In roles as light emitters or in optoelectronic devices, however, a significant barrier to their development has been the finding of photoluminescence (PL) quantum yields typically limited to 1% or lower in solution-phase environments,[4,5] and at best rising to ∼10%.[6,7] Overcoming this limitation requires modifying the fundamental exciton photophysics of SWCNTs, with strategies being provided by considering the evolution of the excitons generated through photoexcitation.[8,9] One critical property is that excitons in the 1D environment of the carbon nanotube (CNT) are highly mobile.[10] As a result, exciton diffusion drives efficient interaction with quenching sites distributed along the nanotube length that act to promote rapid non-radiative relaxation.[4,5,11] Furthermore, the band-edge (E_{11}) exciton produces a manifold of states in which emission from the lowest energy state (lying ∼10 meV lower in energy than the bright emitting state) is formally forbidden.[12] It is estimated that ∼90% of excitations result in excitons populating this dark state,[5] setting an upper bound of ∼10% as an intrinsic limit to PL quantum yield. Routes to overcoming both extrinsic and intrinsic limitations will therefore include improvements in nanotube quality, approaches to optimizing the exciton environment,[13–15] limiting diffusive transport of excitons, and ultimately will also require strategies for conversion of dark states into emitting states.

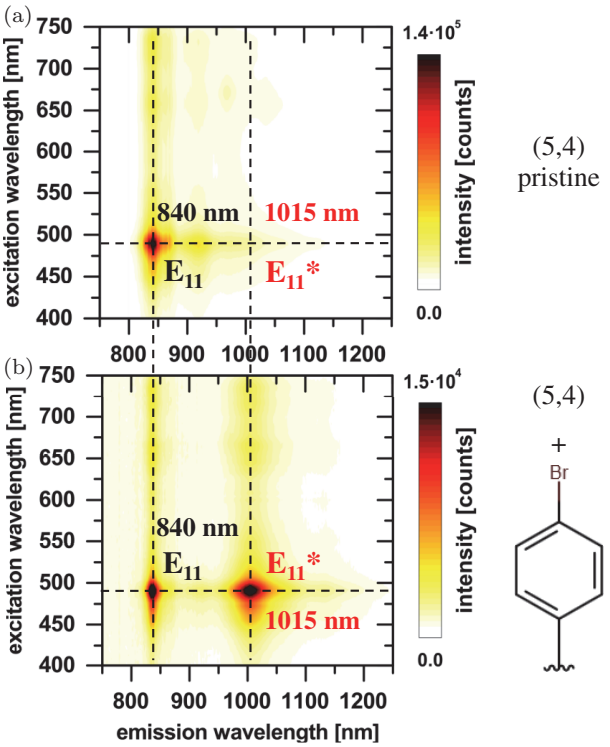

Fig. 1. (a) PL excitation map for unfunctionalized (5,4) CNTs in 1% aqueous sodium deoxycholate. E_{11} emission wavelength at 840 nm. (b) PL excitation map for (5,4) CNTs functionalized with 4-bromobenzene. Defect-state E_{11}^{*} emission wavelength at 1015 nm.

Recent developments in modification of SWCNT optical properties through their covalent functionalization are providing possible answers to the diffusive transport and dark-state conversion problems. Molecular attachment to generate local defect sites in the SWCNT structure is found to create new photoluminescent states (designated here as E_{11}^{*}),[16,17] with energies significantly red-shifted (by ~100–300 meV) from the normal SWCNT E_{11} emission (see Fig. 1). Notably, this red-shifted emission is generated at significantly higher quantum yields (potentially as high as 30%).[16–18] As will be outlined in this chapter, these results indicate that modification of electronic structure at covalent defect sites clearly alters the exciton physics, with exciton localization at defects serving as the origin of new behaviors, while the improved quantum yields must entail some degree of dark-state conversion. It is important to recognize that covalent introduction of photoluminescent defects imparts properties that are significantly different, and brings distinct advantages, in comparison to other

types of photoluminescent defects in SWCNTs. As a prominent example, charge doping to produce trions results in much weaker PL,[19–21] while covalent defects are naturally more chemically stable and are open to a broad range of synthetic tunability towards control of emission properties.

Covalent defects thus present significant new opportunities for expanding SWCNT functionalization chemistry, for exploring a wide range of new photophysics arising from the defects, and for introducing new functionality that emerges only as a direct consequence of exciton localization. This chapter begins with a review of progress in chemistry of the covalent dopants, provides a description of experimental and theoretical efforts towards understanding the electronic structure that arises at the defect sites, and provides an outline of the origin of defect-state emission in diffusive trapping of excitons, with discussion of several behaviors supporting this idea of exciton localization. Localization is then presented as a source of new SWCNT functionality, with a particular emphasis on the potential of covalently introduced defect states to act as quantum emitters at room temperature and at telecom wavelengths. The discussion finishes with an overview of open questions and outlook for future work.

2. Functionalization Chemistry

2.1. *Oxygen-based defects*

Recognition of the potential for covalent defect states to efficiently enhance SWCNT PL properties was initiated by Ghosh *et al.*[16] In their work, SWCNT functionalization with oxygen groups was demonstrated by exposing aqueous surfactant suspensions of SWCNTs to ozone, either by direct bubbling or via injection of ozonated water, with the latter providing more control over reaction extent. Ozonide formation was directly followed by light illumination to promote formation of the stable oxygen adduct. While the reaction mechanism is not yet well understood, its dependence on wavelength suggests photoactivation of an initial adduct as a critical step, with the role of SWCNT photoexcitation remaining an open question. Chemical access to the SWCNT surface was found to be maintained by surfactant coatings of sodium dodecyl or tridecyl benzene sulfonate,[16,18] while the more protective surface coating provided by sodium deoxycholate (DOC) prevents functionalization.[22–24] Optimization of defect-state PL intensities requires ensuring that functionalization only occurs at a low level, with over-functionalization resulting in loss of defect-state and E_{11} PL, as well as bleaching of the SWCNT absorbance spectrum. At low levels of functionalization, the SWCNT absorption spectrum

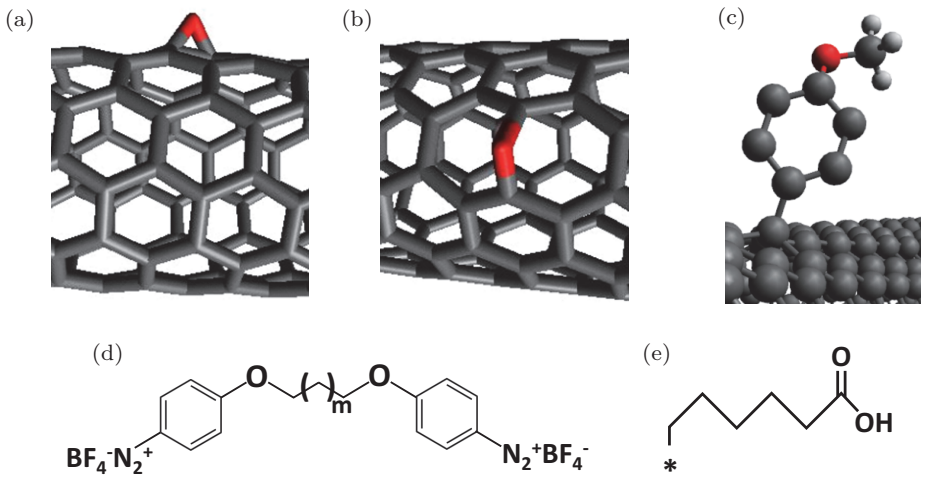

Fig. 2. Examples of SWCNT functionalization agents: (a) epoxide-*l* oriented along the SWCNT axis,[16] (b) ether-*d* oriented perpendicular to the SWCNT axis,[16] (c) 4-methoxybenzene,[17] (d) multipoint binding aryl diazonium reagent,[32] and (e) $-(CH_2)_5COOH$.[38]

is not significantly impacted.[16] Ghosh *et al.* demonstrated ozonation of 10 different SWCNT chiralities, with E_{11}^* energy shifts from E_{11} ranging from 106 to 214 meV as the SWCNT diameter decreases.[16] In the specific case of the (6,5) structure, the defect-state spectrum is dominated by emission at 1120 nm, with weaker features appearing at greater red-shifts (at ~1200–1300 nm). Modeling of possible chemical functionality arising from SWCNT ozonation indicates that ether groups are the likely origin of the primary E_{11}^* emission feature, with epoxides likely responsible for the more red-shifted states (see Figs. 2(a) and 2(b)).[16,22]

Alternative approaches to oxygen functionalization have also been explored. A solid-state route, in which SWCNTs deposited on a substrate are exposed to reactive oxygen species generated by electron-beam bombardment of SiO_2 or Al_2O_3, effectively introduces oxygen functionality while also improving emission stability.[25] Interestingly, the solid-state functionalization incorporates a more balanced population of ether and epoxide groups. While the epoxide is thermodynamically less favored than ether,[16,22] the resultant solid-state matrix that encapsulates the nanotubes in this process may stabilize and thus increase the population of epoxide groups. Notably, the solid-state approach is fully compatible with optoelectronic device fabrication methods. Air-suspended SWCNTs directly exposed to ozone are also known to exhibit enhanced PL,[26] while photo-oxidation of lipid wrapping groups may lead to SWCNT

functionalization following formation of lipidhydroperoxides.[27] Finally, small diameter SWCNTs are susceptible to accidental oxygen functionalization during typical solution-phase processing, due to the high-degree of curvature and built-in strain of their sidewalls.[28]

2.2. sp^3 defects

Greater control and tunability of defect-state emission properties are being realized through introduction of so-called sp^3 defects into the SWCNT sp^2 lattice. While suggested theoretically,[29,30] such a strategy was first demonstrated experimentally through use of aryl diazonium reagents (Fig. 2(c)) in the work of Piao *et al.*[17] The ability to introduce bright emitting states through reactive diazonium reagents contrasts with early diazonium functionalization of SWCNTs, where defects were introduced at high concentrations and known to bleach optical properties.[31] Such behavior again underscores the importance of low-level functionalization to generate defect-state emission. As with oxygen defects, defect density can be controlled by either limiting the concentration of reactive species,[17] or by capping the nanotube surface with a protective layer (by using DOC, for example) once a desired defect density is achieved.[23,24] Estimated quantum yields for sp^3 defect-state emission are as high as 30% and can reportedly be a factor of 10 greater than that found for oxygen defects (depending on aryl species). Such high yields are an indicator that dark diffusive exciton states are likely being converted to the emissive localized defect states. E_{11}^* red-shifts from E_{11} range from ~100 meV to as high as 250 meV, depending on SWCNT diameter.[17] Significantly, red-shifts can be tuned through aryl synthetic modification, with substitution of more electron-withdrawing groups generating larger shifts. This behavior highlights the significant potential to control emissive properties of defects via synthetic modification of the functionalization agents. Beyond simple mono-aryl structures, Shiraki *et al.* have introduced more complex diazonium agents capable of multipoint binding (Fig. 2(d)).[32]

Expansion of sp^3 defect functionality is possible through reductive alkylation of SWCNTs,[33–35] which can also introduce photoluminescent defect states.[36,37] Alkyl and aryl halides provide additional strategies for introducing more complex structures (Fig. 2(e)),[38,39] with fluorene substitution of alkyl hydrogens demonstrated as one effective route to enhancing electron-withdrawing character of dopants for greater red-shifting of PL.[38] Both alkyl bromide and alkyl halide reagents are also capable of introducing true divalent binding species, for which attachment at two adjacent carbon sites can result.[38,39] Alkyl carboxylation has also been demonstrated as an effective route to introducing trion states of the sp^3 defects.[40]

2.3. *Photochemical Control*

As indicated by the role of light in promoting the SWCNT ozonation chemistry,[16] photochemistry can play an important role in controlling introduction of the covalent defects. Light has also been shown to effectively accelerate the diazonium reaction chemistry.[41] Resonant excitation of the SWCNT exciton transitions can promote aryl defect introduction, likely through a photothermal mechanism. The enhancement of the aryl-diazonium reaction rates through sample illumination is also an important route to functionalization of large-diameter SWCNTs, whose decreased curvature may otherwise limit reactivity.[42] Photothermal control has also proven effective in isomerization of diazoether reagents to drive transformation from an inert to reactive form.[43] Such photoisomerization provides an additional route to adding new functionality while introducing the advantage of photoswitchable chemistry.

2.4. *Chemical tuning of spectral features*

A wide range of SWCNT functionalization agents are thus available for introducing photoluminescent defect states (Fig. 2), with significant potential for further development. While synthetic variability can yield progressively tunable changes in defect-state emission wavelengths, it is also found that different

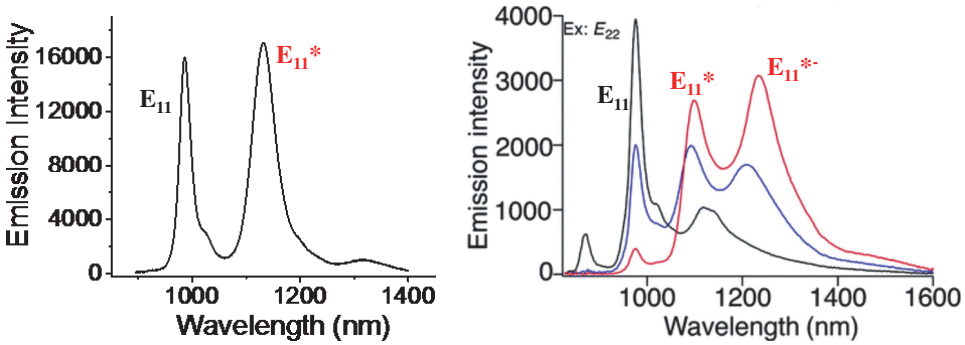

Fig. 3. (a) PL spectrum of 4-methoxybenzene functionalized (6,5) SWCNTs in 1% DOC. (b) PL spectra of unfunctionalized (6,5) SWCNTs (black trace), and *n*-butyl (red and blue trace) functionalized (6,5) SWCNTs in 1% aqueous sodium dodecyl benzene sulfonate (SDBS), showing both E_{11}^{*} and more strongly redshifted E_{11}^{*-} defect-state emission bands. (b) adapted with permission from Ref. 39. Copyright 2016, The Royal Society of Chemistry.

molecular structures can generate entirely different emission bands. As examples, emission induced by simple aryl and alkyl binding can be dominated by a single band occurring at moderate red-shifts from E_{11} (Fig. 3(a)).[17,38] More complex species, however, will generate two emission bands at moderate (E_{11}^{*}) and strongly (E_{11}^{*-}) red-shifted positions (Fig. 3(b)), with relative intensity of the two defect bands depending on specifics of dopant structure.[32,37,39] Such diversity in spectral behaviors provides a route to expand the wavelength range of defect-state emission, but represents a challenge for establishing uniformity of response required for applications. An understanding of the underlying basis for such tunability and variability in spectral behaviors is required for their control and can be established through an evaluation of how defect-state electronic structure is determined by dopant molecular structure and binding to the SWCNT surface.

3. Defect-Site Electronic Structure

The new optical behavior of the covalently introduced emitting states raises several questions about their origin and nature, which include the need to confirm exciton localization at defect sites, understand the localization mechanism, identify the chemical functionality linked to a given spectroscopic behavior, and determine the associated electronic structure. To address the latter points, a successful strategy has been to pair low-temperature spectroscopic studies with electronic structure modeling of the emergent defect states.[22,44]

3.1. *Spectroscopic probing of defect-state electronic structure*

Recent low-temperature, single-tube PL spectroscopy studies performed on oxygen-[22] and aryl-functionalized SWCNTs[44] show that the defect states indeed emit sharp, isolated spectral lines at the positions of the prominent defect band observed in room-temperature (T) ensemble PL spectra. In addition to these sharp peaks, which provide direct confirmation of localization of excitons to quantum dot (QD)-like states, the low-T single tube spectra revealed many interesting features that are buried in ensemble room-T PL spectra. These features shine the first light onto the chemical nature of the defects and their electronic fine structure.

In Fig. 4, low-T emission spectra of individual (6,5) SWCNTs functionalized with oxygen[22] and 4-methoxy benzene[44] are compared side by side. While a single sharp isolated peak is observed in the 980 ± 30 nm range of the low-T PL spectra of individual pristine (6,5) SWCNTs for the emission of the E_{11}

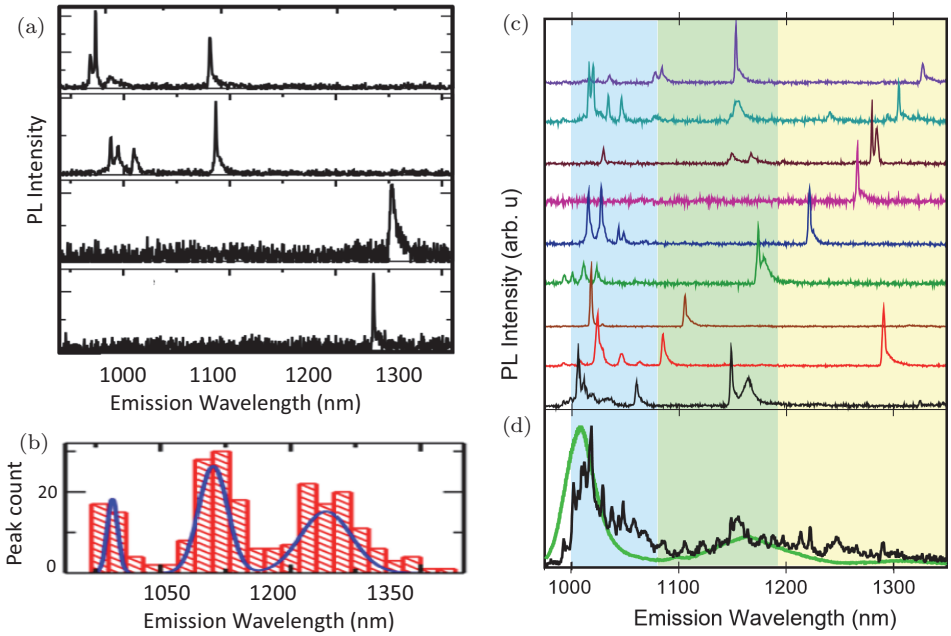

Fig. 4. Low-temperature PL spectra of individual oxygen (a) and aryl defects (c) in (6,5) SWCNTs. (b) Histogram showing PL peak distribution of oxygen defects (red bars) and Gaussian fit (blue curve). (d) Average of 60 low-temperature PL spectra of individual aryl-functionalized SWCNTs (black) and room-temperature PL spectrum of aryl-functionalized SWCNTs in solution (green). Adapted with permission from Refs. 22 and 44. Copyright 2014 and 2017, respectively, American Chemical Society.

band edge exciton, the spectra of both types of functionalized SWCNTs show sharp emission peaks distributed in the 1000–1300 nm spectral range. In some SWCNTs (1st and 2nd spectra of Fig. 4(a) and 6th and 9th spectra of Fig. 4(c)), sharp emission peaks from the E_{11} band can also be observed together with the defect-state emission. Interestingly, in those cases the E_{11} emission appears split into 2–3 peaks, indicating that introduction of aryl and oxygen defects not only introduces deep trap states but also splits the E_{11} transition.

While PL spectra of individual oxygen and aryl-functionalized SWCNTs appear very similar, the distribution of the defect-state emission peaks differs significantly. In (6,5) SWCNTs, the PL peaks of individual oxygen defects group into two inhomogeneously broadened distributions centered at 1120 and 1250 nm, with a FWHM of ~60 nm (Fig. 4(b)), suggesting that oxygen functionalization creates at least two different types of deep trap states. On the other hand, an average of more than 60 PL spectra of individual aryl-functionalized (6,5) SWCNTs (Fig. 4(d)), shows defect emission peaks

distributed continuously in the 1000–1300 nm spectral range. This spectral diversity indicates that aryl functionalization leads to significantly more different types of deep trap states than in the case of oxygen functionalization. These findings can be understood through quantum chemical modeling of the defect states.

3.2. *Quantum chemistry modeling*

Modeling-wise, atomistic quantum chemical simulations, such as methodologies based on density functional theory (DFT), are currently able to provide semiquantitative estimates of alteration of electronic structure in pristine carbon nanotubes caused by chemical functionalization. Here the researcher faces two challenges: The first fundamental problem is that the underlying precise geometries and conformations of binding sites are unknown for specific spectroscopic data. Consequently, investigations of multiple chemically viable binding configurations and establishing relationships between calculated electronic structure features and experimental spectra significantly broaden theoretical studies and bring an uncertainty to theory/experiment comparisons.

Secondly, conceptually, one needs to adopt either periodic boundary conditions or a finite size model of the tube. In the former, considering the numerically tractable small unit cell size containing the chemical defect will lead to spurious interactions between periodic replicas and effectively represents the case of very large and perfectly ordered defect concentration, a situation well beyond the experimental conditions. Moreover, modeling of external perturbations such as dielectric medium or solvent effects is not straightforward in this case. Here, periodic boundary condition modeling via the solution of the Bethe–Salpeter equation by adding self-energy corrections (GW) to the DFT has been widely successful for the case of pristine tubes,[45–47] but has rarely been used to model chemical functionalization. Alternatively, one may use a finite tube segment as an input to electronic structure simulations,[48,49] thus adapting methodologies previously developed for molecular materials. This approach has a number of advantages, such as freedom of simulating any desirable geometry of a tube functionalized with one or a few defects. Beyond addressing realistic defect concentration, it is conceptually simple to account for electron–phonon coupling, local disorder, external field, and dielectric environment effects. However, unsaturated chemical bonds at the open tube ends have to be capped with hydrogen atoms and methylene (CH_2) groups to remove midgap states caused by dangling bonds.[50] Moreover, long tube segments typically exceeding 10 nm should be used in the simulations to avoid artifact effects of quantum confinement. Stated differently, the length of nanotube segments

must be chosen to be significantly larger than the diameter of the tube and characteristic exciton sizes (about 5 nm). Such limitations necessitate simulating systems with 1000 or more atoms, which inevitably imposes restrictions on the DFT model and basis set used for finite systems.

In the following examples, simulations were performed with finite tube segments 10–12 nm in length, typically containing over 1000 atoms and terminated with hydrogen atoms at all edge positions to passivate dangling bonds. As a model, quantum chemistry hybrid DFT models such as B3LYP or CAM-B3LYP functionals were applied and coupled with the STO-3G basis set. Hybrid DFT is important due to reduction of self-interaction errors and its ability to account for excitonic effects,[51] whereas use of a small basis set allows one to reduce numerical expense without significant impact on accuracy.[52] Furthermore, the dielectric environment of solvents can be introduced via polarized continuum models, without noticeable increase in numerical expense. DFT simulations provide energies and geometric structures for the ground state, whereas time-dependent DFT (TD-DFT) modeling assesses the same quantities for electronically excited states and evaluates spectroscopic properties.

These calculations provide an explanation for several of the defect-state experimental findings noted in Section 3.1.[22,44,52] In the case of oxygen functionalization of (6,5) SWCNTs, DFT calculations reveal that out of five possible configurations for oxygen functionalization (ozone-l, ozone-d, ether-l, ether-d, and epoxide-l, where -l/-d represent C-O-C bond aligned parallel/perpendicular to the (6,5) tube axis), only ether-l, ether-d, and epoxide-l (Fig. 5(a)) are stable and create defects with the lowest emission states at 1023, 1100, and 1284 nm (Fig. 5(b)). The experimentally observed distributions centered at 1120 and 1250 nm are in excellent agreement with the calculated transitions for ether-d and epoxide-l. In addition, a more careful analysis of experimental data based on peak distribution as a function of energy shift from the E_{11} transition reveals a small peak distribution centered at the ether-l transition.[22]

With aryl functionalization, the bound aryl group is accompanied by a reactive electron located on a nearby SWCNT carbon atom.[30,44,52] The excess electron site can capture a proton or an OH group, leading to two carbon atoms on the SWCNT surface formally adopting sp^3 hybridization. The bound proton or OH group can be located either adjacent to the site of the initial aryl addition ("ortho") or three carbon atoms away (para). As a result, aryl functionalization can lead to six distinct configurations, labeled as ParaL30, OrthoL-30, OrthoL90, ParaL90, OrthoL30, and ParaL-30 ("±30" and "90" stands for the approximate angle between aryl-H;/OH arrangement and the (6,5) tube

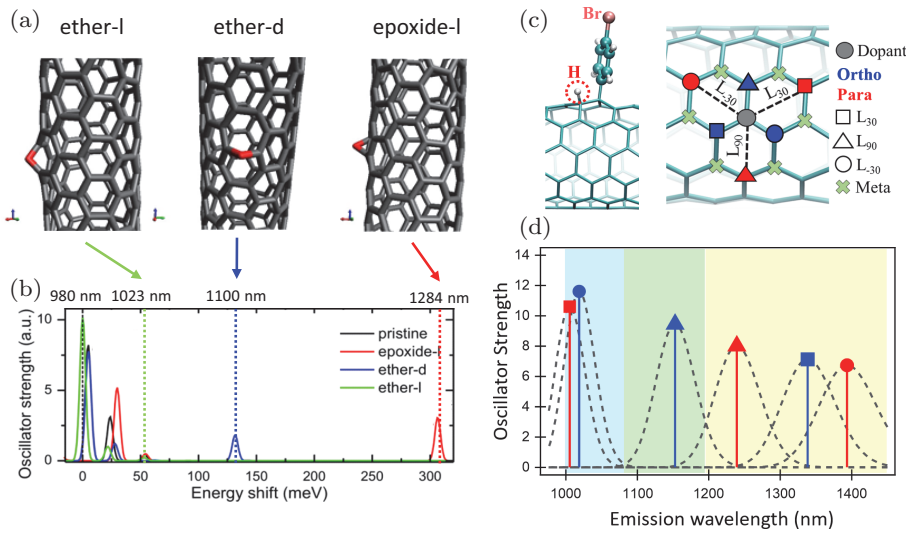

Fig. 5. (a) Three stable binding configurations on (6,5) SWCNTs for oxygen functional groups: ether-l, ether-d, and epoxide-l, where -l(-d) represent O–C–O bond direction aligned parallel(perpendicular) to the tube axis. (b) Optical transitions for pristine (unfunctionalized, black) (6,5) SWCNTs, ether-l (green), ether-d (blue), and epoxide-l (red) configurations, with the lowest energy states at 980, 1023, 1100, and 1284 nm, respectively. (c) Side view of aryl-H defect (left) and six distinct aryl-H binding configurations (right) on (6,5) structure. (d) Lowest energy emitting transitions of six configurations marked in the same notation as in (c). Adapted with permission from Refs. 22 and 44. Copyright 2014 and 2017, respectively, American Chemical Society.

axis) (Fig. 5(c)). In contrast to the case of oxygen functionalization, DFT calculations for (6,5) aryl-H functionalization show that all six configurations are equally likely to occur, with the lowest emissive states at 1005, 1019, 1153, 1239, 1338, and 1393 nm (Fig. 5(d)). Because multiple transitions fall within the possible inhomogeneous distribution of each other, it becomes impossible to assign a specific experimentally observed peak to a particular transition, as in the oxygen case. However, qualitative agreement between the spread of calculated transitions and the observed spectral range in which the PL peaks are distributed suggests that the existence of six distinct chemical configurations is the root cause of the spectral diversity. In addition to explaining the spectral peak distribution, the calculations also show that symmetry breaking, resulting from the introduction of defects, in both cases leads to brightening of the dark states located near E_{11}, thus providing an explanation for the observation of splittings in the E_{11} transitions (Fig. 5(b)).

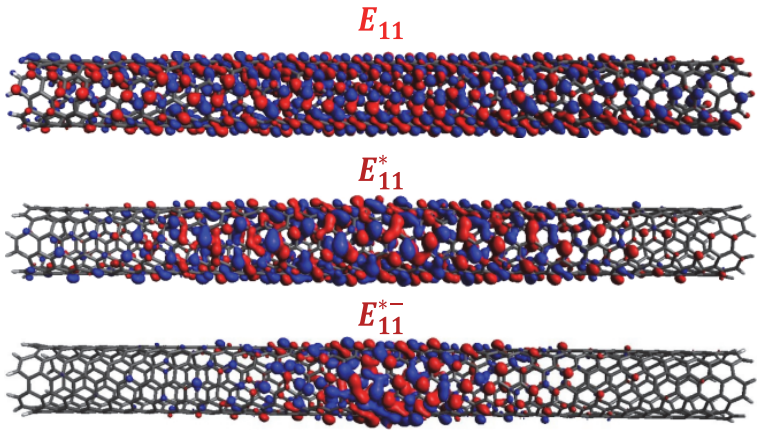

Fig. 6. The spatial distributions of transition densities for E_{11} (pristine tube), E_{11}^{*} (ether-d defect), and E_{11}^{*-} (epoxide-l) electronic states on (6,5) structure. The electrons and holes are represented in red and blue, respectively. While E_{11} excitons in pristine CNTs are delocalized, E_{11}^{*} and E_{11}^{*-} excitons exhibit increasing localization with an increase of trapping energy. Adapted with permission from Ref. 22. Copyright 2014, American Chemical Society.

Further insight into the distribution of the excitonic wavefunction over the nanotube can be achieved by examining the orbital delocalization of the transition densities associated with their parent electronic states.[22,44,52] Importantly, for all defect-state cases considered, their excited state wavefunctions are distributed over some surface of the nanotube through the π-conjugated orbital network. The atoms of the molecular adduct do not directly participate; however, the defect presence perturbs the π-electrons locally, leading to formation of new low-lying electronic states. Moreover, it is observed that an increased trapping energy is always concomitant with increased exciton localization. Thus, deeper traps correspond to more localized states (as illustrated in Fig. 6) with reduced oscillator strength, in line with physical intuition.

3.3. *Reorganization energy: Role and evaluation*

An important consequence of localization of the excited state excitonic wavefunction is modification of electron–phonon coupling. Owing to a relatively rigid structure and delocalized states, electron–phonon coupling in pristine SWCNTs is relatively weak compared to molecular materials, which nevertheless is well determined experimentally and captured via simulation.[53] Localization of electronic states due to defects significantly amplifies changes of the π-electron density in the excited state as compared to that in the ground state,

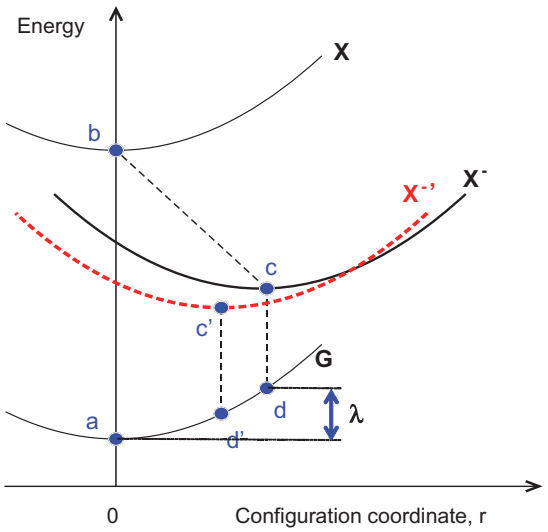

Fig. 7. Reorganization energy is related to the displacement between potential energy surfaces, where ground (G), trapped exciton (X−), and free exciton (X) refer to different electronic states. "Configuration coordinate" *r* (horizontal axis) denotes the deformation (reorganization) of the SWCNT geometry. The reorganization energy (λ) is dominated by displacement of nuclear coordinates. The red curve for a trapped exciton ($X^{-\prime}$) delocalized over two defect sites illustrates change in reorganization energy due to defect concentration. Adapted with permission from Ref. 54. Copyright 2016, American Chemical Society.

which leads in turn to increased electron–phonon (or electron–vibrational) coupling strength. Consequently, geometries of the ground and defect-introduced electronic states become different, and excited state structural deformation can be characterized with a so-called reorganization energy, dominated by displacements of nuclear coordinates (graphically depicted in Fig. 7). This vibronic relaxation of excited states has profound consequences on the carrier dynamics involving trapping and de-trapping of excitons at the defect sites.[54] In particular, this phenomenon may appear as a substantial mismatch between optical energy gap and thermally determined de-trapping energy (line bc, Fig. 7). Here, the optical gap is defined as a difference in emission energies between the native exciton (line ab, Fig. 7) and defect trap states (line cd, Fig. 7), whereas the defect de-trapping energy is related to a capacity of the exciton to escape the trap thermally, and can be determined by application of the van't Hoff equation.[16,54] Experimentally determined reorganization energies in a series of fluorescent aryl defects incorporated in semiconducting SWCNTs can be as large as 100 meV, and are strongly dependent on the defect density.[54] These

experimental findings agree well with the results of DFT simulations, which allow one to map the observed trends into dopant-dependent vibrational reorganization energy in the molecular picture.[54]

4. Exciton Localization at Defect Sites

The low-T spectroscopic results, paired with DFT theory, thus directly imply a mechanism for defect-state emission in which initial optical excitation of E_{11} excitons is followed by their diffusive transport to and trapping at covalently introduced defect sites. Theoretical modeling indicates exciton transition density becomes localized to a 3–5-nm region centered on the defect sites, with deeper traps expected to generate a higher degree of localization (Fig. 6).[22,44,52] Upon trapping, the exciton takes on the electronic structure associated with the particular defect and emits accordingly (Fig. 8). The structure and functionality of the molecular dopant, as well as its binding configuration or orientation at the nanotube surface are both important factors in determining defect-state emission wavelengths. A critical aspect of this model is thus the concept of exciton localization. It is the ultimate origin of the basic photophysics of the SWCNT defects, while also being an essential feature for introducing new SWCNT functionality. With the critical role played by localization, it is valuable to consider the range of experimental evidence supporting this behavior.

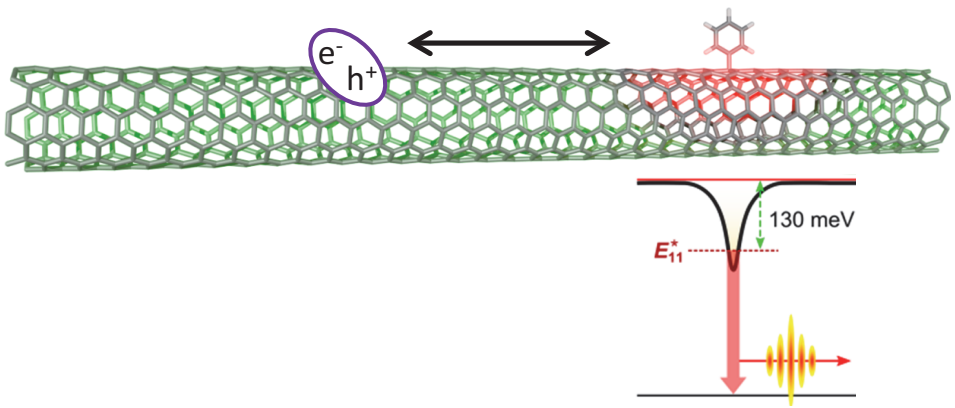

Fig. 8. Depiction of defect-state excitation and emission processes. Optical excitation creates a band-edge (E_{11}) exciton ($e^{-}h^{+}$) that freely diffuses until trapped at the aryl defect site (130 meV trapping potential as shown). The localized exciton then emits according to the electronic structure of the specific defect.

4.1. *Photoluminescence imaging of exciton localization*

The most direct evidence for exciton localization at defect sites comes from correlated simultaneous 2-color PL imaging of individual functionalized SWCNTs.[23] In this approach, E_{11} and E_{11}^* PL is imaged at their respective emission wavelengths on separate imaging channels and subsequently combined into a single positionally correlated image. An example of such an image is shown in Fig. 9(a) for a methoxybenzen-functionalized (6,5) SWCNT. In the PL image, E_{11} emission (shown in green) is observed over continuous stretches of the nanotube. In contrast, defect-state emission (E_{11}^*, shown in red) appears at highly localized positions on the nanotube. The 2D spatial distribution of the defect-site emission spots (Fig. 9(b)) indicates that their emission extent is within the 210-nm resolution of the imaging instrumentation.[23] Such localization behavior has been confirmed for both oxygen and sp^3 aryl defects.[23]

Notably, a comparison of the spatial distribution of E_{11} and E_{11}^* PL intensities (Fig. 9(c)) shows that, wherever an emitting defect site exists, it corresponds to a significant decrease in E_{11} intensity at the same location. This behavior is a

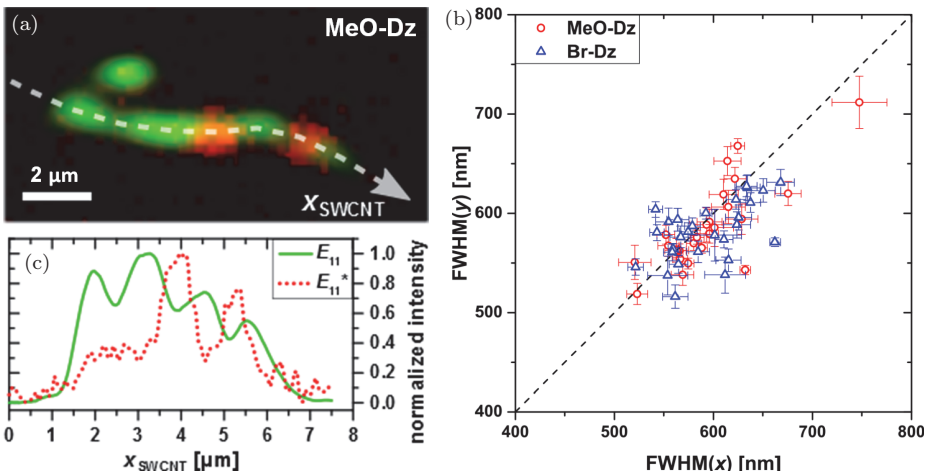

Fig. 9. (a) PL image of a single (6,5) SWCNT functionalized with 4-methoxybenzene. E_{11} emission (at 985 nm) in green, with localized defect-state (at 1120 nm, E_{11}^*) emission in red, showing two separate defect sites. (b) Transverse (y) and axial (x) 2D Gaussian imaging widths of defect-site PL spots obtained from PL images of (6,5) SWCNTs functionalized with 4-methoxybenzene (red points) and 4-bromobenzene (blue points). The black dashed line indicates a direct $y = x$ correlation. (c) PL intensity distribution along the length (as indicated by the white dashed arrow) of the SWCNT in (a) for E_{11} (green) and E_{11}^* (red) emission. Adapted with permission from Ref. 23. Copyright 2015, The Royal Society of Chemistry.

strong indicator that the E_{11} exciton is being converted to the trap state of the defect site. Moreover, the E_{11} intensity distribution around the defect site can be analyzed within a model of 1D exciton diffusion. The fall-off in E_{11} intensity around the defect site can be fit to diffusive behavior with an average exciton diffusion length of 200 nm.[23] Such a value agrees well with expectations for exciton diffusion lengths in unfunctionalized SWCNTs.[5] Taken together, the direct PL imaging results strongly support the idea of diffusive exciton trapping at the covalently introduced defect sites.

4.2. *Intrinsic spectral characteristics of localized excitons*

Low-T single-tube PL spectroscopy provides another clear evidence of exciton localization, namely, sharp isolated PL peaks characteristic of 0D quantum

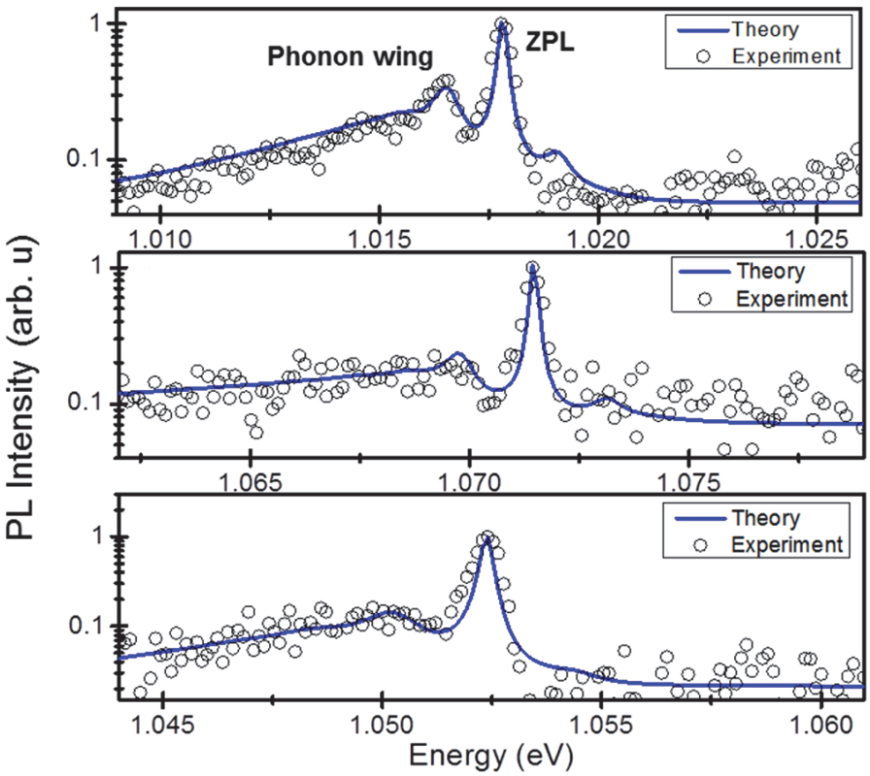

Fig. 10. High-resolution PL spectra of three individual aryl-functionalized, PFO-Bpy wrapped (6,5) SWCNTs (black circles) and calculated spectra (blue lines) based on coupling between localized acoustic phonon and defect-bound excitons. The spectra are shown in a semi-log plot to show the acoustic phonon side band clearly. Adapted with permission from Ref. 44. Copyright 2017, American Chemical Society.

dots. Oxygen defect states emit PL peaks with an average FWHM of 6.38 ± 3.46 meV with a minimum FWHM of 3 meV.[22] The sharpest spectral lines, with FWHM of 270 μeV, were observed on aryl defect states of SWCNTs wrapped in PFO-BPy.[44] More interestingly, PL peaks of both aryl and oxygen defects exhibit a peculiar asymmetric broadening that can also be observed in emission of E_{11} band-edge excitons.[55–58] Specifically, sharp PL peaks are broadened only on the low energy side. Strength and shape of the low energy band vary from one peak to another. When the low energy band is weak and separated from the main peak by a small energy gap of a few meV, the main peak appears symmetric and exhibits the narrowest linewidths (Fig. 10, bottom). Sometimes, multiple weak peaks were observed in the low-energy band, together with a weaker high energy side peak (Fig. 10, top). These line shapes were also observed in the case of E_{11} band-edge excitons when the SWCNTs were well isolated from the environment by wrapping in PFO-BPy.[57] The work on E_{11} band-edge excitons explained these line shapes in terms of coupling between excitons localized in a shallow potential fluctuation and 1D acoustic phonons experiencing varying degrees of confinement. Following this work, the asymmetrically broadened peaks of Fig. 10 are explained as the result of coupling between 1D free acoustic phonons and a defect-bound localized exciton. The peculiar line shapes of Fig. 10 are explained using a model that considers the interplay between defect-bound excitons and localized acoustic phonons.[44,57] The model reproduces all the key features of the spectral lines when the confinement length for the acoustic phonons is varied between 5 and 28 nm, while keeping the exciton confinement length between 3.4 and 3.6 nm and the acoustic-phonon barrier height of 1.3–1.5 meV nearly constant. The exciton confinement length of 3.4–3.6 nm is in good agreement with the $\sim 2.7-3.9$ nm orbital distribution of the transition densities for the four lowest energy aryl-H configurations found by quantum chemistry computation.[44,52]

4.3. *Stability of exciton localization*

Localized excitons of various material systems enable many technologies, ranging from next-generation photovoltaic cells and low-threshold lasers to quantum light sources. All of these applications hinge upon the ability of a localized exciton to maintain its quantum mechanical characteristics. Material systems with a shallow confinement potential (e.g., InGaAs QDs, 2D transition metal dichalcogenides) can maintain exciton localization only at cryogenic temperatures.[59–61] Due to their confinement potentials being hundreds of meV deep, the SWCNT defect states can maintain exciton localization up to room

T. This point is evident in recent room-T single photon generation experiments (see Section 5.2). In addition to the depth of the trap potential, spectral isolation from other nearby states is also very important. For example, in the case of InGaAs QDs,[59,60] while QDs emit sharp isolated spectral peaks at low excitation powers, PL peaks of multiexciton states, as well as the emission tail of the band-edge exciton, rise up as backgrounds that reduce the single photon purity. Pump-dependent low-T PL spectra of SWCNT aryl as well as oxygen defects show that defect-state emission spectra are free of such background emission over more than two orders of magnitude variation in pump power (Fig. 11(a)). A plot of the integrated PL intensities of the E_{11} band-edge exciton and defect-state emission bands (Fig. 11(b)) show that while the intensity of the defect-state emission band strongly saturates and quenches at high pump

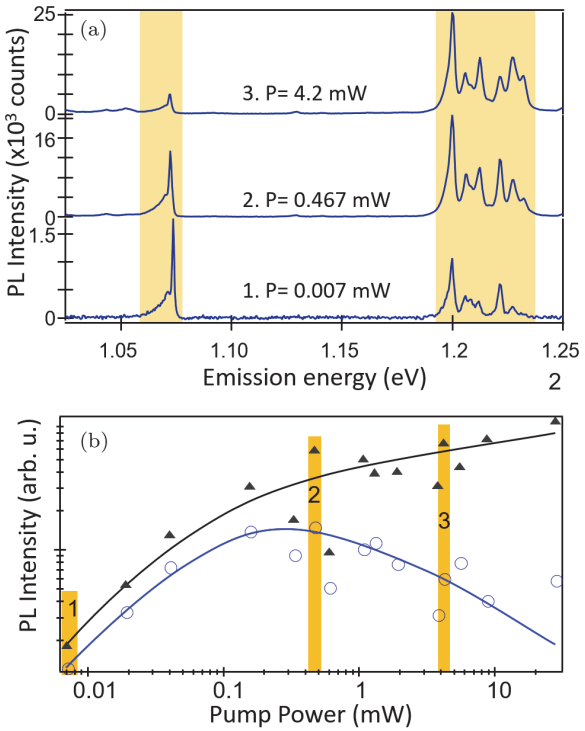

Fig. 11. (a) Pump dependent PL spectra of an individual aryl-functionalized (6,5) SWCNT, showing that the defect band remains spectrally isolated from the band-edge emission for more than 2 orders of magnitude variation in pump power. (b) Integrated PL intensity of defect emission band (blue circles) and band-edge exciton band (black triangles) plotted as a function of pump power. The defect and band-edge emission bands are marked in (a) with yellow bands. Adapted with permission from Ref. 44. Copyright 2017, American Chemical Society.

fluence, the E_{11} emission band shows only a moderate saturation. A similar nonlinear behavior has also been observed for single tubes as well as in ensembles for oxygen defects.[22,62] While the quenching of the defect-state PL may indicate photoinduced damage, strong saturation of the defect-state PL can be attributed to rapid ground-state depletion of the local states caused by an efficient accumulation of photogenerated free excitons into the sparse local states through 1D diffusional migration of excitons along the nanotube axis.[62] These findings suggest that defect-states may be able to assist in achieving population inversion, necessary for lasing, which has been hampered in intrinsic SWCNTs owing to rapid exciton–exciton annihilation processes.

4.4. *Relaxation dynamics*

4.4.1. *Diffusive trapping*

The short PL lifetimes ($\sim$10−50 ps), typically observed for E_{11} exciton relaxation, are understood as a consequence of exciton diffusion,[4,5] which allows rapid access to quenching centers (including nanotube ends) to provide an efficient means of nonradiative relaxation. Similarly, the presence of covalently bonded defect sites will provide centers for removal of E_{11} exciton population. Thus, if the defect density were to increase, the E_{11} exciton lifetime is expected to decrease as a consequence of diffusive trapping. Hartmann *et al.*[24] have demonstrated this behavior by measuring PL lifetimes for a series of (6,5) SWCNTs in which the defect density was controllably increased (see Fig. 12(a)). In agreement with expectations, the results showed that the E_{11} lifetime rapidly decreases as the defect density increases (Fig. 12(b)).[24] These results add support for the picture of diffusive trapping as a populating mechanism for the E_{11}^{*} defect states.

It is important to note that the E_{11} PL decay is usually biexponential, and the above discussion concerns the behavior of the faster component of the decay, which has been attributed to non-radiative relaxation of the bright E_{11} exciton state.[63–66] A significantly weaker ($\sim$few percent) slow decay component ($\sim$150−200 ps) is interpreted as the relaxation time for the lower-lying dark exciton state.[63–66] Interestingly, the dark-state decay times (Fig. 12(b)) also become shorter as the defect density is increased. As with the bright exciton, this result indicates that the dark E_{11} exciton also undergoes diffusive trapping at the defect sites. This is an important result in that dark-state trapping is a prerequisite for conversion of dark excitons into bright emitting defect states as a route to boosting quantum yields. While the PL lifetime results do not definitively show conversion of dark-to-bright states, they at least show that this first step in the conversion process does occur.

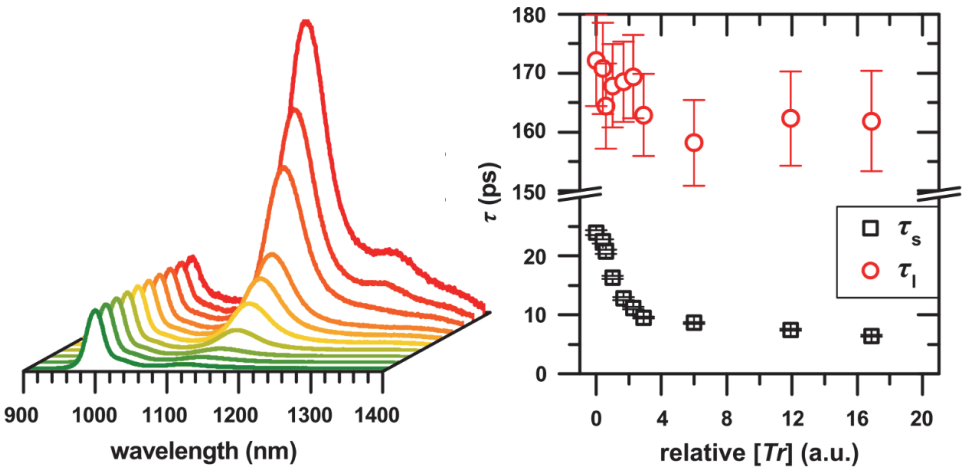

Fig. 12. (a) PL spectra of 3,5-dichlorobenzene-functionalized (6,5) SWCNTs as defect density is increased (green to red). All spectra normalized to E_{11} intensity at 985 nm. (b) Short (τ_s, black points) and long (τ_l, red points) lifetime components of E_{11} PL decay, plotted as a function of relative defect density as represented in graph (a). Adapted with permission from Ref. 24. Copyright 2016, American Chemical Society.

4.4.2. *Localized exciton dynamics*

Examples of defect-state PL decay curves for functionalized (5,4) and (7,5) SWCNTs are shown in Fig. 13. As for the E_{11} exciton, the defect-state decays are also found to be biexponential, but with two significant differences. The defect-state lifetime components are closer in time scale (with short (τ_s^*) and long (τ_l^*) components of 215 and 608 ps, respectively, for (5,4) and 24 and 82 ps, respectively, for (7,5)).[24] Additionally, the weights of the components are more similar: 30% (70%) for the short (long) component for (5,4) and 56% (44%) for the respective components of the (7,5) defect-state decay. This behavior is consistent with defect-state population relaxing from two discrete electronic levels. This is in agreement with the theory results discussed above, which indicated that the defect-state excitons can also exist as either bright or dark states. Miyauchi *et al.* also found that T-dependent spectra for oxygen-functionalized SWCNTs could be understood by invoking a dark defect state lying at lower energy than the bright emissive state.[18]

Because the two decay components are similar in time scale and amplitude, it is not possible to assign either component to decay of a specific state. Instead, the rate at which the ratio of the populations in the two states changes can be considered on characteristic time scales (see Fig. 14). At long time scales, fast

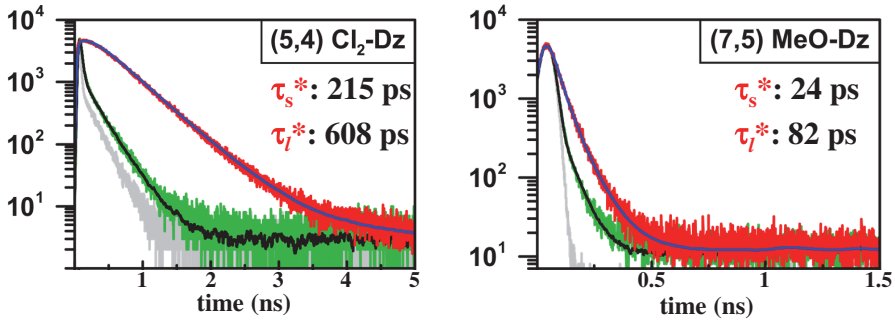

(a) (b)

Fig. 13. (a) E_{11} (832 nm, green) and E_{11}^* (1,014 nm, red) PL decay curves for 3,5-dichlorobenzene-functionalized (5,4) SWCNTs. (b) E_{11} (1035 nm, green) and E_{11}^* (1,190 nm, red) PL decay curves for 4-methoxybenzene-functionalized (7,5) SWCNTs. Short (τ_s^*) and long (τ_l^*) lifetime components of the biexponential defect-state (E_{11}^*) decays are highlighted in each case. Adapted with permission from Ref. 24. Copyright 2016, American Chemical Society.

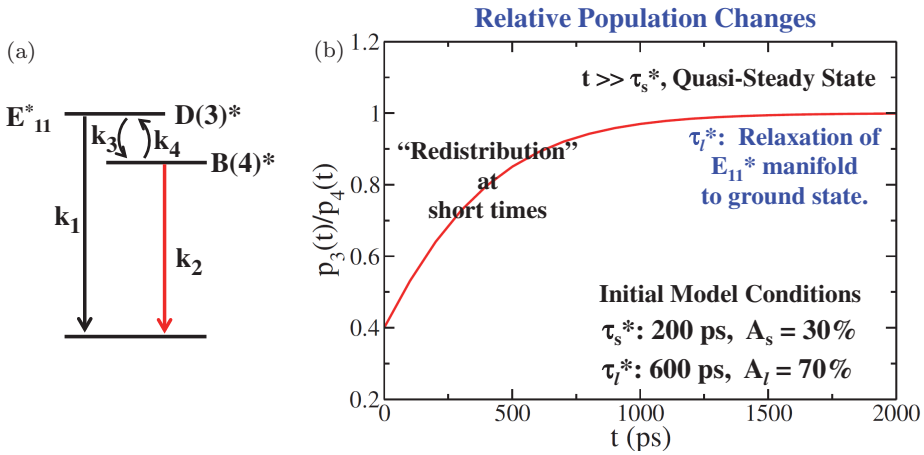

Fig. 14. (a) Energy level schematic for E_{11}^* manifold of dark (D(3)*) and bright (B(4)*) localized exciton states, with decay rates (k_1 and k_2) for relaxation to the ground state and population exchange (k_3 and k_4) between the bright and dark defect states. (b) Illustration of how population redistribution process (τ_s^*) and population relaxation to the ground state (τ_l^*) translate to varying ratio of dark state ($p_3(t)$) and bright state ($p_4(t)$) populations after initial photoexcitation. Assumed model parameters are given as inset to plot and are similar to typical expectations for functionalized (5,4) SWCNTs.[24]

processes (governed by τ_s^*) will effectively be complete. The relative populations after this point remain constant, even while the overall defect-state manifold will decay to the ground state. At shorter times, the initial populations must then evolve to these long-time "steady-state" ratios. This process is considered to be one of population redistribution, and has a time scale of τ_s^*. Given this result, τ_l^* must then reflect the time scale for decay of the defect-state manifold to the ground state. With the long lifetime component being that for ultimate population decay, the remaining discussion focuses on its behavior.

Inspection of defect-state decay in Fig. 13, in comparison to that for E_{11} excitons, clearly shows that defect-state lifetimes are longer (typically by a factor of 5–10).[18,24] Such extension of relaxation times is expected as a direct consequence of exciton localization,[18,24] which will prevent the diffusive quenching inherent to the E_{11} decays. The extended PL lifetimes thus serve as another confirmation of exciton localization at defects. Miyauchi *et al.* also find that the enhanced radiative recombination resulting from such localization plays a significant role in yielding the enhanced quantum yields found for the defect states.[18]

Also apparent in Fig. 13 is a strong SWCNT chirality dependence in observed defect-state lifetimes. In general, as the nanotube diameter is increased, the PL lifetime is found to decrease,[24] which can be understood as a consequence of the structural dependence of the defect-state emission energies. As seen in Fig. 15, PL decay times increase significantly as the defect-state

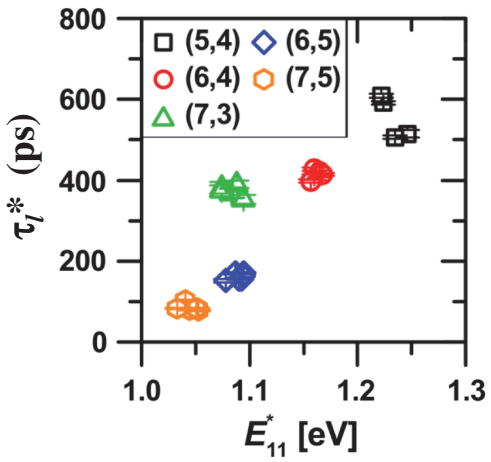

Fig. 15. Plot of long defect-state (E_{11}^*) PL decay component (τ_l^*) as a function of emission energy for (5,4) (black), (6,4) (red), (7,3) (green), (6,5) (blue), and (7,5) (orange) SWCNTs. Adapted with permission from Ref. 24. Copyright 2016, American Chemical Society.

emission energy increases. This behavior is indicative of a multiphonon relaxation mechanism, in which larger energy gaps will require an increased number of phonon interactions to bring the system to the ground state, and thus entail longer relaxation times. Multiphonon decay time scales on the order of 100s of picoseconds to nanoseconds had been predicted in early theoretical work,[67] but the behavior was previously masked by the high rate of diffusive exciton quenching processes. When localization effects are accounted for in determining the associated exciton–phonon coupling, theoretical decay rates are found to be in close agreement with those found experimentally.[24,54,67]

5. New Functionality Through Defects

5.1. *Multifunctionality for sensing and imaging*

Beyond introducing new SWCNT photophysics, exciton localization at defects is an essential part of using defects to impart new functionality. Interest in SWCNTs as photoluminescent imaging agents originates in their near-infrared PL falling within a window of transparency in biological environments.[68] Of particular interest offered by defect-state PL is the ability to do imaging based on E_{11} excitation and using E_{11}^* emission for detection. This approach avoids the biological auto-fluorescence that can plague imaging based on excitation at visible wavelengths, while harnessing the strong E_{11} absorption cross-section. The result is a marked increase in imaging contrast.[16,68] An alternative imaging approach can be based on recently discovered photon upconversion.[39,69,70] Akizuki *et al.* have demonstrated that the covalent defect states can be populated through direct excitation at the E_{11}^* transition energy.[69] Thermal detrapping of the trapped exciton creates E_{11} excitons that subsequently emit at higher energy than the original excitation (photon upconversion). Demonstration that the upconversion intensity increases as the temperature increases further supports the idea of thermal detrapping from defect states as the origin of the E_{11} emission.[69] The upconversion functionality is thus a direct consequence of initial exciton formation and localization at the defect sites. With both excitation and emission wavelengths in the near-infrared (with emission this time on the high-energy side of excitation) high contrast imaging is again demonstrated.[69,70]

Exciton localization at defect sites also introduces the potential for multifunctionality. Localization forces a more direct interaction between the exciton and whatever other functionality may be built into the molecular structure of the chemical dopant. As examples of using this strategy towards sensing applications, analyte binding at, or analyte-driven chemical modification of the defect site can change its emitting properties.[71,72] This concept has been

demonstrated as an effective route to SWCNT-based pH sensing, in which defect-site binding of protons can shift E_{11}^{*} emission wavelengths.[71] Additionally, saccharide binding to boronic acid functionality of phenylboronic acid-bound defect sites can also shift E_{11}^{*} emission wavelengths, effectively demonstrating molecular recognition at defect sites as a novel route to glucose and fructose sensing.[72]

5.2. *Room temperature quantum emitters*

Quantum emitters, materials capable of single photon emission, are of growing interest for optically-based approaches to quantum information processing, security, and computing, quantum photonics, and ultrasensitive metrology and sensing applications.[59,73–75] Of particular interest are systems capable of operation at room temperature and emitting at telecom wavelengths (1.3–1.5 μm) to facilitate integration into fiber-based photonic information networks. Pairing of these characteristics in a single material, however, has remained an elusive goal. Room-T response has been attained in color-center materials such as diamond and silicon carbide, but is limited to short wavelength emission in these materials due to their large band gaps.[59,74,75] Telecom wavelength single photon emission has been demonstrated in III–V semiconducting QDs, but only at cryogenic temperatures.[76] Interestingly, localized defect states in low-dimensional materials, including transition metal dichalcogenides[61] and hexagonal boron nitride,[77] are showing some promise as single photon emitters, but again are constrained by temperature and/or wavelength range. With the ability to deterministically introduce covalent defects into SWCNTs, paired with tunability of emission wavelengths based on changes with nanotube diameter[78] and their natural suitability for integration into electro-optic devices,[2] SWCNTs hold significant potential for development as functional single photon sources.

5.2.1. *Antibunching in absence of defects*

Single photon emission (SPE) requires a quantum mechanical two level system, yet the 1D nature of SWCNTs conflicts with this major requirement. SPE, however, becomes possible in SWCNTs due to trapping of excitons to 0D localized states and the strong exciton–exciton interaction of 1D systems. When SWCNTs are deposited on substrates (e.g., glass), small morphological variations of the substrate together with a non-uniform coverage of surfactant molecules or wrapping polymer give rise to microscopic variation in local dielectric environments and hence in the electronic potential of the exciton along the length of the SWCNT. As a result, excitons with sufficiently low kinetic

energy can get trapped in local potential minima. Evidence of such unintentional exciton localization was reported early in optical studies of SWCNTs.[79] The spatial extent of unintentional localizations[80] and depth of their potential wells[81] have since been determined systematically. In 2008, Hogele *et al.* performed Hanbury–Brown–Twiss experiments on such localized states and demonstrated SPE in SWCNTs for the first time.[82] However, because the trapping potentials of such unintentionally localized excitons are very shallow, SPE was realized only at cryogenic temperatures. Moreover, the SPE suffers from random intensity and emission energy fluctuations, as well as photobleaching that results from temporal fluctuations of the dielectric environment, thus limiting SWCNT promise as a material for SPE. Recently, Hofmann *et al.* have shown that localized exciton states formed on CVD-grown SWCNTs suspended across a SiO_2 void are capable of bright SPE free of blinking and spectral diffusion.[83] They also demonstrated ultranarrow spectral linewidths ($<40\,\mu$eV) and long PL lifetimes (>3 ns) indicative of long-lived quantum coherence, which is highly desirable for indistinguishable single photon generation. While this system brings a significant advance in SWCNT-based quantum light generation, its operation is still confined to cryogenic temperatures.

Because SWCNT excitons are confined to 1D, they can collide when they are created close to one another. When two excitons collide, only one survives, with the energy of the other transformed to heat. This process, known as exciton–exciton annihilation (EEA), can in principle lead to a saturation such that multiple excitons created in a SWCNT annihilate one another non-radiatively until only a single exciton remains to emit a single photon in one excitation cycle. Since this scenario does not rely upon exciton localization, it opens an interesting alternative route for room-T single photon generation. Recent reports, however, show that this effect only results in partial SPE, with room-T single photon purity typically lower than 50% (i.e., $g^2(0) > 0.5$)[84,85] and best results ($g^2(0) \sim 0.28$) coming from long, suspended, high-quality CVD grown SWCNTs displaying very long exciton diffusion lengths ($\sim 1\,\mu$m).[86] By correlating the highest single photon purity that can be obtained from a SWCNT with its exciton diffusion lengths, Ma *et al.* showed that attaining SPE in this scheme is highly dependent on a delicate balance between exciton diffusion and EEA processes,[84] with high-purity SPE only possible by limiting exciton creation to a few hundred nanometer region. Similarly, Ishii *et al.* concluded that highly localized exciton generation would be required to obtain room-T SPE in as-produced SWCNTs.[86] Therefore, while a proof-of-principle demonstration of room-T SPE may be possible, it is unlikely to extend this scheme toward effective electrically driven single photon generation. Ma *et al.* further postulated

that EEA processes, working hand in hand with exciton localization capable of surviving to room-T, could lead to room-T single photon generation.[84]

5.2.2. *Defects as route to room-T single photon emission*

As noted above, exciton localization is an essential aspect of attaining room-temperature single photon emission in SWCNTs. Localization provides the required single emitter exhibiting quasi-two-level behavior, with the potential to survive at room T. While localization can occur at shallow accidental traps, sustained trapping at room T requires deep traps (much greater than $k_B T$ at room-T, or 26 meV). The trapping states introduced by covalent functionalization exhibit exactly the characteristics required. Ether and epoxide defects have been shown to provide trapping potentials of 100–300 meV in (6,5) SWCNTs, with the latter providing emission wavelengths at the edge of the telecom O band (1,300 nm).[22]

By exploiting the PL stability afforded through the solid-state functionalization process described in Section 2.1,[25] Ma *et al.* were able to make the first demonstration of room-T SPE from SWCNTs by accessing the oxygen defect-state PL.[87] SPE was demonstrated using a Hanbury–Brown–Twiss experiment to measure the second-order photon correlation function, $g^{(2)}(t)$, for the defect-state emission from cryogenic (4 K) to room (298 K) temperatures. SPE is indicated when $g^{(2)}(t = 0)$ approaches zero (indicating strong photon antibunching), showing a vanishing probability of two or more photons being emitted per excitation cycle. Values less than 0.5 are typically indicative of some level of SPE, while values close to zero indicate higher single-photon purity, defined as $1 - g^{(2)}(0)$. As seen in Fig. 16(a), not surprisingly, at 4 K excellent $g^{(2)}(0)$ values of 0.04 can be obtained from ether defects.[87] Good antibunching is found across the T range, with values of 0.05 and 0.32 at 150 and 298 K, respectively (with the latter obtained from an epoxide defect); see Fig.s 16(d) and 16(g).[87] Notably, in each of the examples, the defect state emission spectrum is found to consist of a single PL peak, indicating that emission is coming from a single defect site. Multisite emission must be avoided to maintain SPE functionality.

As the sample T is increased, the spectral linewidth increases from ~1 meV obtained at 4 K to ~20 meV at room-T (Fig.s 16(b), 16(e), and 16(h)). Over the same range, the E_{11}^* emission intensity rises to a peak at ~200 K then diminishes again at room-T. The intensity behavior can be understood as a combination of two effects. Miyauchi *et al.* suggest that the loss in intensity at cryogenic T is a consequence of a dark defect state lying at lower energy than the emitting state.[18] Intensity may be lost at higher T due to the potential for thermal

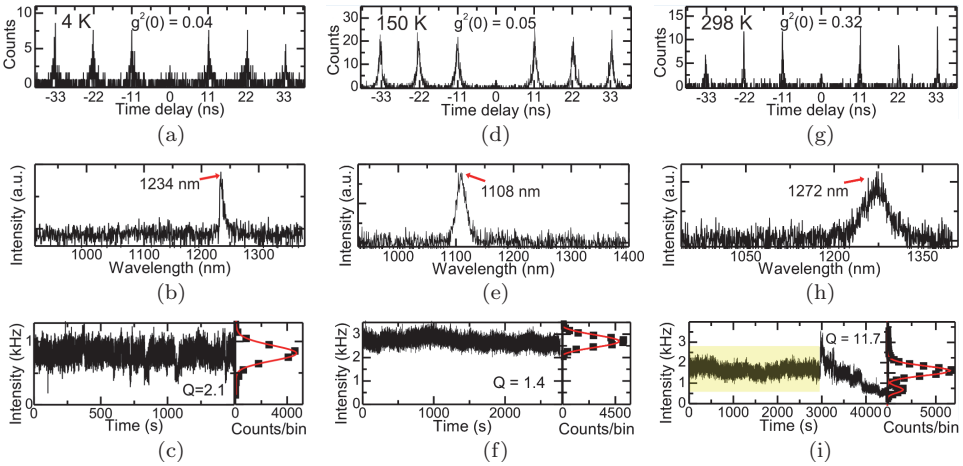

Fig. 16. Second-order photon correlation plots ($g^{(2)}(t)$, top) showing photon antibunching behavior, single-nanotube defect-state PL spectrum (middle), and plot of defect-state PL intensity over time (bottom) taken at (a)–(c) 4 K, (d)–(f) 150 K, and (g)–(i) 298 K, for oxygen-functionalized (ether-*d* and epoxide-*l* emitting states) (6,5) SWCNTs prepared in an SiO_2 matrix. Adapted with permission from Ref. 87. Copyright 2015, Macmillan Publishers Limited.

detrapping of the localized exciton.[69] In parallel, PL lifetimes are also found to decrease at higher T, also likely the result of detrapping, which increases in efficiency with T as an additional non-radiative decay channel. This behavior underscores the importance of confirming the existence of defect dark states and further characterizing them. While PL stability over extended time periods is found to be near shot-noise limited at low T, at room-T significant instability sets in, including jumps in intensity and even blinking (Figs. 16(c), 16(f), and 16(i)).[23,87] The improvements in stability and degree of antibunching found with a modest decrease in T can easily be attained through use of readily available thermoelectric coolers. Alternatively, significant improvements in stability can also be found by incorporating sp^3 aryl defects as the quantum emitter.[23,42]

DFT modeling of oxygen defect sites provides insight into the origin of their PL instability. Such defects are accompanied by a permanent dipole that significantly perturbs the local electrostatic environment of the trapped exciton (see Fig. 17(c)) and can act as an antenna to the environment for promoting charge-induced blinking.[23] In contrast, aryl defects are expected to perturb the electrostatic environment to a much lesser degree (Figs. 17(a) and 17(b)), with the result being reduced blinking, in agreement with experimental PL imaging assessments.[23] By also integrating aryl-functionalized SWCNTs into

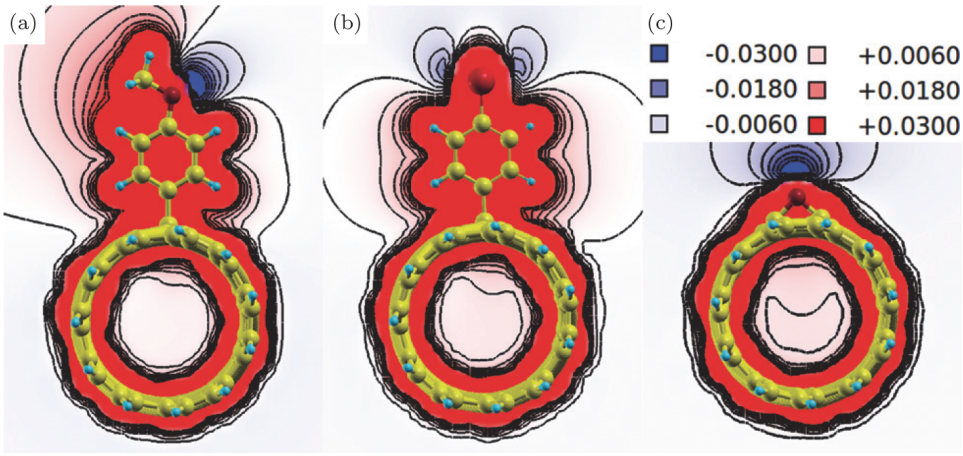

Fig. 17. Calculated electrostatic potential maps associated with a localized exciton trapped at (a) 4-methoxybenzene, (b) 4-bromobenzene, and (c) ether-*d* functionalization sites on a (6,5) SWCNT, and illustrating markedly increased perturbation associated with the oxygen defect site in comparison to the aryl sp^3 defects. Adapted with permission from Ref. 23. Copyright 2015, The Royal Society of Chemistry.

a low-polarity, low-charge environment, significant improvements in defect-state PL stability should be achieved. In addition to improved photophysical behavior, aryl and other sp^3 functionalization of SWCNTs has the benefit of providing routes to synthetic tunability of properties and improved control over extent of reaction,[23,24,42] important in limiting defect sites to one per tube for SPE needs. Furthermore, by using reactive diazonium reagents for functionalization, it becomes quite feasible to incorporate defects into larger diameter SWCNTs (having reduced reactivity due to decreased curvature) as a route to achieving strong PL red-shifting for accessing the telecom C band (at 1500 nm).[16,17,42]

As demonstrated in dichlorobenzene-functionalized (6,5) SWCNTs (Fig. 18), the expected advantages of the aryl sp^3 defects are indeed realized. At room T, PL stability is now shot-noise limited (Fig. 18(c)).[42] Control over functionalization easily translates to single-site doping per tube, as evidenced by a high probability of finding nanotubes with a single defect-state emission peak (Fig. 18(a)). Strong antibunching, with $g^{(2)}(0)$ values of 0.01 are reliably found (Fig. 18(b)).[42] The importance of consistently obtaining nanotubes with a single defect site is illustrated in Fig. 18(d), which shows an example of a tube exhibiting three PL peaks (indicating 3 defect sites). The $g^{(2)}(0)$ value for this nanotube is 0.6 (Fig. 18(e)), close to the theoretical expectation of 0.66 for the case of three independent emitters.

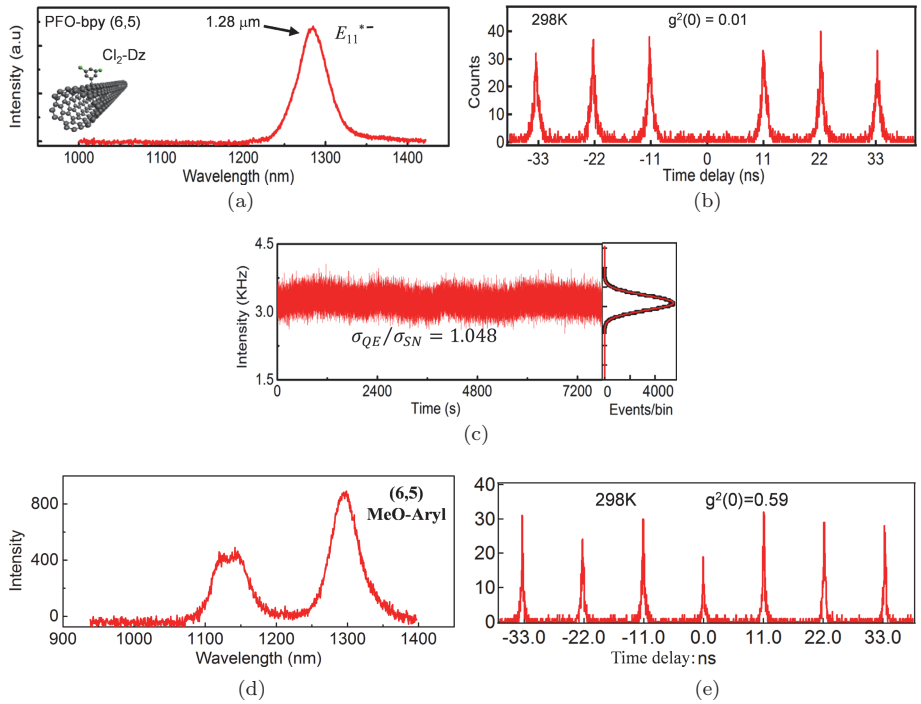

Fig. 18. (a) PL spectrum and (b) corresponding second-order photon correlation ($g^{(2)}$(t)) plot and (c) defect-state PL intensity over time for a single PFO-polymer wrapped (6,5) SWCNT functionalized with 3,5-dichlorobenzene. (d) PL spectrum of a single 4-methoxybenzene-functionalized (6,5) SWCNT showing emission features from three distinct defect sites. (e) Corresponding second-order photon correlation plot with $g^{(2)}(0)$ value of 0.59, confirming photon emission arising from three defect sites. All data taken at 298 K. (a)–(c) adapted with permission from Ref. 42. Copyright 2017, Macmillan Publishers Limited.

A significant advantage available with SWCNTs as SPEs is that emission wavelengths are tunable by selecting SWCNTs of differing diameters.[78] The principal for structural tunability of defect-state PL is illustrated in Fig. 19(a), which shows the energy level structure for band-edge and defect exciton states for three SWCNT structures varying in diameter from 0.76 to 0.83 to 0.94 nm (for (6,5), (7,5), and (10,3) structures, respectively). As the diameter increases, the E_{11} emission energy decreases from 1.26 to 0.98 eV. In parallel, the defect-state emission energy decreases as well. As seen in Fig. 19(b), defect states in (6,5) will span wavelengths from 1140 to 1300 nm, (7,5) spans 1180 to 1330 nm (encompassing the telecom O band), and (10,3) emits from 1370 to 1580 nm (covering the telecom C band). As discussed above in Section 3, the span of emission wavelengths for each chirality is too broad to originate

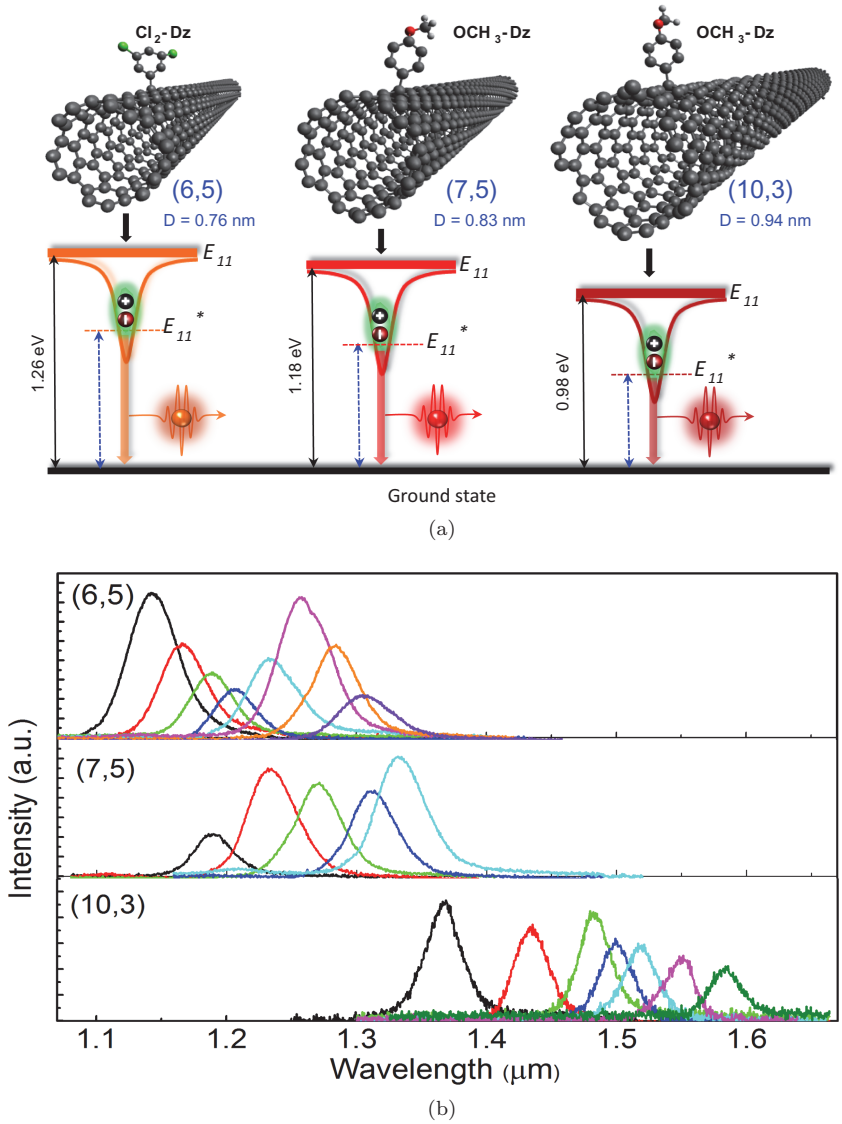

Fig. 19. (a) Principle of SWCNT diameter-dependent tuning of defect-state emission wavelength. As diameter (d_t) increases from (6,5) (d_t = 0.76 nm) to (7,5) (d_t = 0.83 nm) to (10,3) (d_t = 0.94 nm), both band-edge (E_{11}) and localized defect-state (E_{11}^*) exciton emission wavelengths become progressively redshifted. (b) Example defect-state spectra obtained from (6,5) (top), (7,5) (middle), and (10,3) (bottom) SWCNTs, functionalized with 3,5-dichlorobenzene or 4-methoxybenzene, as per (a). Broad range of emission wavelengths for each structure arises from multiple binding configurations available to the aryl sp^3 defect, as discussed in Section 3.[42,44] Each spectrum obtained from different single nanotubes at room temperature. Adapted with permission from Ref. 42. Copyright 2017, Macmillan Publishers Limited.

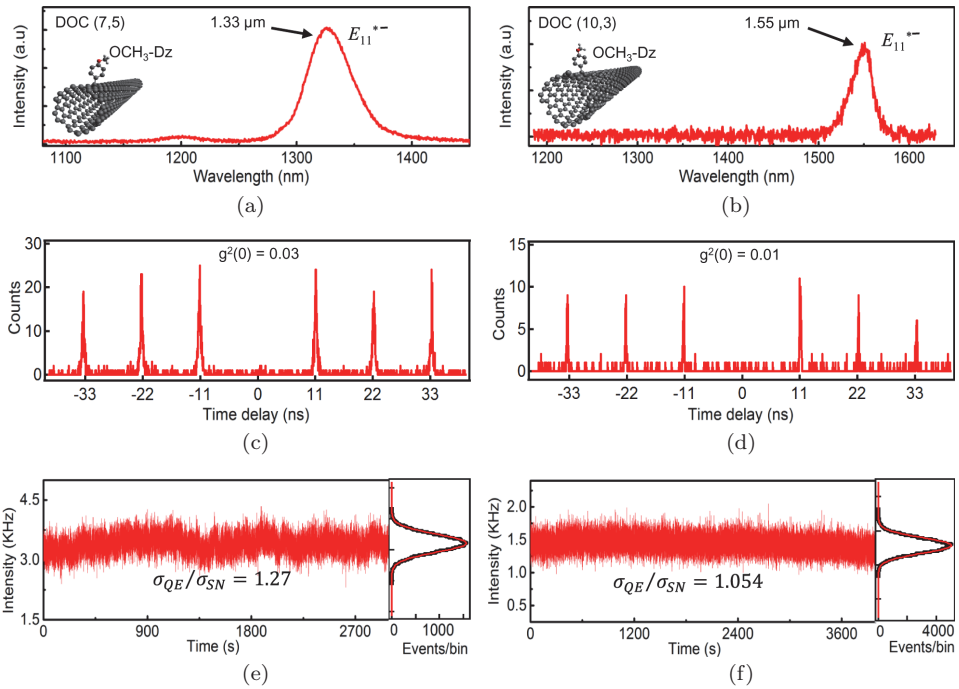

Fig. 20. Single-nanotube defect-state PL spectra (a) and (b), second-order photon correlation plots ($g^{(2)}(t)$), (c) and (d) showing strong photon antibunching behavior, and plot of defect-state PL intensity over time (e) and (f) taken for a single (a) (7,5) and (b) (10,3) SWCNT at room-temperature. Adapted with permission from Ref. 42. Copyright 2017, Macmillan Publishers Limited.

from environmental effects alone, but instead arises from the range of bonding configurations available from the aryl diazonium reaction chemistry used in the functionalization process. Of particular interest is the ability to harness the variety of bonding configurations to produce strongly red-shifted states that allow defect-state emission at telecom wavelengths with select nanotube diameters.

As already demonstrated for the (6,5) chirality, both (7,5) and (10,3) structures also exhibit the ability to support single defect sites per tube, with each providing shot-noise limited PL stability at room T (Fig. 20).[42] Most importantly, the (7,5) SWCNTs reliably provide strong antibunching at wavelengths centered around 1300 nm, while the (10,3) SWCNTs display excellent antibunching values at the heart of the most commonly used telecom wavelength: 1,550 nm (Fig. 20).[42] These outstanding characteristics have been demonstrated across multiple chiralities, using different aryl dopants, and under both surfactant and polymer wrapping conditions.[42] This behavior places functionalized SWCNTs as the only current material able to act as single-photon

emitters at room T and at telecom wavelengths. Notably, SPE count rates are $\sim 2-3$ times higher than obtained from oxygen defect states, and when collection efficiency and detector sensitivity are accounted for, the defect state quantum emitters can yield SPE count rates on the order of 10^5 to 10^6 photons per second, approaching rates available with the most efficient emitters currently under study.[42] Given this unique functionality of the SWCNT defect-state emission, development of SWCNT defects as effective single-photon sources will continue to be a promising direction for future efforts.

6. Future Directions

6.1. *Opportunities in defect chemistry*

There remain significant opportunities to explore, understand, and control defect state behaviors introduced by covalent functionalization of SWCNTs. Advances to date have harnessed relatively simple oxygen, aryl, and alkyl dopant structures. There exists, however, a vast synthetic space for generating more complex defect functionalities. Existing diazonium and reductive halide chemistries can form the basis for expanding structural types.[32,38] Additionally, adding new reactive species, such as diazo and diazoether,[43] can form the basis for new functionality, adding additional control over reactivity, tuning of emission wavelengths, and defining multi-defect interactions through defined defect placement. It will also be important to push beyond the predominantly aqueous chemistry currently used for functionalization. Of particular importance is developing strategies for efficient functionalization of polymer-wrapped SWCNTs suspended in organic solvents like toluene. Such a capability will expand the potential for integrating functionalized SWCNTs into optical and electronic device structures and enable their use in a diversity of forms and matrices.

The concept and development of covalent defects as multifunctional light emitters is in its infancy. The potential of engineered defects to act as binding sites or probes for enhanced sensing,[71,72] when paired with the quantum emitter aspect of the defect states, holds potential for applications in quantum metrology. Co-localization of catalytic functionality may lead to more efficient photocatalysts. Addition of heavy metals for promoting spin-orbit coupling, or induced generation of trions,[40] can add spin functionality to the defect sites as a route to added dimensionality in information processing. Defect sites might also be designed that enhance conversion of dark diffusive excitons to emitting trap states as a means to further boost PL quantum yields.

6.2. *Open questions in defect-state photophysics*

Despite the recent advances in understanding the origins and behaviors of defect-state PL, its photophysics remains wide open for exploration. Of tremendous importance for further improvement of quantum yields is gaining an improved mechanistic picture of exciton localization at defects, with a focus on evaluating the extent to which dark excitons are converted to emitting defect states and the role played by phonons and SWCNT chirality in that process. Additionally, a deeper understanding is required of defect-state electronic structure, particularly confirming the presence of localized dark excitons and other exciton states (such as triplets), their relative energy ordering,[18,54] and whether that ordering and interconversion of states can be controlled by selection of chirality, influence of the molecular dopant, or application of external perturbations. A significant complement to electronic structure studies will be the comprehensive determination of defect-state relaxation pathways, including elucidation of mechanisms and dynamics of interconversion between states and thermal detrapping. Concerning the goal of developing emitters of indistinguishable photons, the intrinsic limits of defect-state PL lifetimes, spectral linewidths, and dephasing mechanisms remain to be determined. Improved understanding of many of these photophysical processes will feed directly into design principles for new chemical structures of the molecular dopants.

Multiple quantum optical experiments are also necessary to achieve understanding and control of the quantum coherence properties of the defects. Specifically, single-photon quantum interference experiments[88] would be very powerful for investigating the competition between spectral diffusion and exciton–phonon coupling in defining the intrinsic linewidth of the defect emission. Ultimately, Hong–Ou–Mandel experiments would be needed to demonstrate single-photon indistinguishability. It is also important to perform these experiments under resonant optical excitation to explore coherent generation of indistinguishable single photons that fully inherit the coherent properties of the excitation laser.[89–91] Such coherent single photons with highly superior indistinguishability have been demonstrated in InGaAs self-assembled QDs[59,60] and could further enable quantum interference experiments, forming the basis of linear optical quantum computation and distant entanglement schemes.

6.3. *Strategies for manipulating defect-state PL*

There is a significant potential for further enhancement of defect-state emission properties, including boosting effective quantum yields, narrowing of

spectral linewidths, and manipulating emission directionality, through integration into photonic, plasmonic, and metamaterials structures.[92] The principles for such enhancement have already been demonstrated in a number of cases for unfunctionalized SWCNTs, as well as on other low-dimensional optical nanomaterials. Straightforward extension of these strategies for coupling to functionalized SWCNTs should be feasible. Resonant confinement of light in optical micro(nano) cavities to strengthen light-matter interactions has been demonstrated to significantly narrow SWCNT emission linewidths, while also boosting emission intensities in microdisks,[93] photonic crystal cavities,[94] and in nanobeam dielectric and air-mode cavities.[95] Fabry–Pérot cavities, in which the optical emitter is placed between dielectric mirrors, have been significantly improved in recent developments to allow efficient and tunable coupling of SWCNT emission to cavity modes.[96,97] Use of such cavity-integration strategies with functionalized SWCNTs may be a productive route towards higher single-photon emission count rates and line widths narrowed sufficiently to attain photon indistinguishability for quantum information needs.

Coupling of SWCNTs to plasmonic nanoantennae can enhance radiative emission rates and thus PL intensities.[98–100] In particular, SWCNTs incorporated at the vertices of bow-tie antenna structures have exhibited quantum yields of ~70% and ultranarrow linewidths (~20 μeV) at 4 K.[100] Strong light-matter coupling to generate exciton-polaritons has also been demonstrated for CNTs integrated with plasmonic disk arrays.[101,102] In addition to expanding the range of exotic photophysics obtainable from SWCNTs, such integration may lead to polariton-based lasing that could be extended to SWCNT defect states. Plasmonic nanodisc structures also can be designed to promote directional light emission for enhanced photon capture.[103,104] Such emission directionality may also be obtained through integration to dielectric antenna arrays.[105,106]

Integration of SWCNT defect states into photonic/plasmonic cavities is the key to success of these strategies. Yet, to date, most of the experiments mentioned above have relied upon single-basis fabrication or even random hit or miss approaches to achieve coupling. The chance of success for such an approach further decreases for defect states because one requires not only that a nanotube, but also the single defect site in that nanotube, becomes precisely aligned with the plasmonic/photonic cavity. Therefore, a deterministic approach capable of coupling defects to a cavity with precision and repeatability is especially needed. Towards that goal, in addition to traditional microelectronic fabrication approaches, one must explore emerging nanolithography approaches, including dip-pen nanolithography, self-assembly, and 3D nanoprinting technologies. Furthermore, instead of relying solely on

solution-based functionalization approaches, development of approaches for deterministic placement of defects in prefabricated SWCNT-cavity coupled structures is also necessary. This deterministic placement of defects needs to be explored not only via covalent chemistry, but also via ion implantation approaches.

6.4. *Integrated opto-electronic devices*

A key need for quantum information applications is a photon source capable of generating single photons "on demand". Electroluminescent (EL) devices are preferred in this case, as individual elements can be controllably addressed and can be integrated into massively parallel devices. Due to their 1D nature, SWCNTs are natural elements for integration into nanoelectronics and have previously been established as EL emitters at both the single-tube level[107,108] and in thin-film devices.[109,110] SWCNT EL devices are also now well positioned for direct integration into complex photonic circuitry. A number of advances in their development have shown their direct pairing with optical waveguides,[111] coupling to nanobeam photonic cavities,[112] and electrically driven SPE at cryogenic temperatures observed through direct coupling to

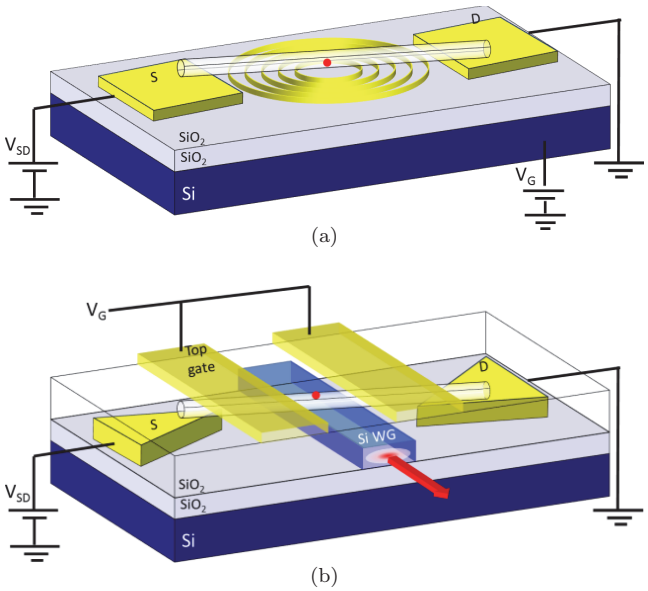

Fig. 21. Schematics of electrically driven single photon sources integrated with bulls-eye structure for collimated emission (a) and Si waveguide for further integration into photonic/plasmonic integrated circuits (b). The red dot represents a deterministically placed defect.

ultrafast superconducting nanowire detectors.[113] Electrically driven exciton-polariton devices have also been demonstrated.[114] Demonstration of SWCNT defects as EL emitters will be an important first step towards opening the full potential afforded by EL device advances and integration to a range of photonic enhancement mechanisms (Fig. 21). The defect integration approach mentioned in the previous section will also play a key role in achieving this ultimate goal.

7. Conclusion

In this chapter, we have explored developments in generation, optical properties, and promising emergent functionalities of CNT defect states created through low-level covalent functionalization of the nanotube sidewall. The defect-state behaviors have great potential for overcoming the challenges presented by the intrinsic nature of the diffusive band-edge excitons, providing a route to optimally harness the PL response of the nanotubes. While significant advances have already been demonstrated in developing a range of molecular dopants, there remains tremendous opportunity to devise innovative routes for control of defect-state properties and to introduce additional functionality through synthetic tunability of these agents. Defect alteration of the nanotube electronic structure leads directly to the wavefunction localization phenomena underlying the observed PL behaviors. Critical fundamental questions, however, remain to be addressed, including revealing the details of how diffusive excitons are converted to the localized states and what is the ultimate fine structure of the defects. The dynamics and mechanisms associated with all processes remain open for study. The new defect-state functionalities are sure to lead to novel application areas, with significant interest and opportunity for development arising from their quantum emission behaviors at room T and telecom wavelengths. Paired with emerging developments in the manipulation of SWCNT PL emission via photonic and plasmonic arrays, with further integration to optoelectronic devices, SWCNT defects are poised to play a unique role in quantum photonics.

References

1. Zhang, M.; Atkinson, K. R.; Baughman, R. H. Multifunctional carbon nanotube yarns by downsizing an ancient technology. *Science* **2004**, *306*, 1358–1361.
2. Avouris, P.; Freitag, M.; Perebeinos, V. Carbon nanotube photonics and optoelectronics. *Nat. Photon.* **2008**, *2*, 341–350.

3. O'Connell, M. J.; Bachilo, S. M.; Huffman, C. B.; Moore, V.; Strano, M. S.; Haroz, E. H.; Rialon, K. L.; Boul, P. J.; Noon, W. H.; Kittrell, C.; Ma, J.; Hauge, R. H.; Weisman, R. B.; Smalley, R. E. Band gap fluorescence from individual single-walled carbon nanotubes. *Science* **2002**, *297*, 593–596.
4. Hertel, T.; Himmelein, S.; Ackermann, T.; Stich, D.; Crochet, J. Diffusion limited photoluminescence quantum yields in 1D semiconductors: Single-wall carbon nanotubes. *ACS Nano* **2010**, *12*, 7161–7168.
5. Crochet, J. J.; Duque, J. G.; Werner, J. H.; Lounis, B.; Cognet, L.; Doorn, S. K. Disorder limited exciton transport in colloidal single-wall carbon nanotubes. *Nano Lett.* **2012**, *12*, 5091–5096.
6. LeFebvre, J.; Austing, D. G.; Bond, J.; Finnie, P. Photoluminescence imaging of suspended single-walled carbon nanotubes. *Nano Lett.* **2006**, *6*, 1603–1608.
7. Tsyboulski, D. A.; Rocha, J.-D. R.; Bachilo, S. M.; Cognet, L.; Weisman, R. B. Structure-dependent fluorescence efficiencies of individual single-walled carbon nanotubes. *Nano Lett.* **2007**, *7*, 3080–3085.
8. Wang, F.; Dukovic, G.; Brus, L. E.; Heinz, T. F. The optical resonances in carbon nanotubes arise from excitons. *Science* **2005**, *398*, 838–841.
9. Maultzsch, J.; Pomraenke, R.; Reich, S.; Chang, E.; Prezzi, D.; Ruini, A.; Molinari, E.; Strano, M. S.; Thomsen, C.; Lienau, C. Exciton binding energies in carbon nanotubes from two-photon photoluminescence. *Phys. Rev. B* **2005**, *72*, 241402(R).
10. Cognet, L.; Tsylbouski, D.; Rocha, J.-D. R.; Doyle, C. D.; Tour, J. M.; Weisman, R. B. Stepwise quenching of exciton fluorescence in carbon nanotubes by single-molecule reactions. *Science* **2007**, *316*, 1465–1468.
11. Harrah, D. M.; Swan, A. K. The role of length and defects on optical quantum efficiency and exciton decay dynamics in single-walled carbon nanotubes. *ACS Nano* **2011**, *5*, 647–655.
12. Perebeinos, V; Tersoff, J.; Avouris, P. Radiative lifetime of excitons in carbon nanotubes. *Nano Lett.* **2005**, *5*, 2495–2499.
13. Ju, S.-Y.; Kopcha, W. P.; Papadimitrakopoulos, F. Brightly fluorescent single-walled carbon nanotubes via an oxygen-excluding surfactant organization. *Science* **2009**, *323*, 1319–1323.
14. Lee, A. J.; Wang, X.; Carlson, L. J.; Smyder, J. A.; Loesch, B.; Tu, X.; Zheng, M.; Krauss, T. D. Bright fluorescence from individual single-walled carbon nanotubes. *Nano Lett.* **2011**, *11*, 1636–1640.
15. Duque, J. G.; Oudjedi, L.; Crochet, J. J.; Tretiak, S.; Lounis, B.; Doorn, S. K.; Cognet, L. Mechanism of electrolyte induced brightening of single-wall carbon nanotubes. *J. Am. Chem. Soc.* **2013**, *135*, 3379–3382.
16. Ghosh, S.; Bachilo, S. M.; Simonette, R. A.; Beckingham, K. M.; Weisman, R. B. Oxygen doping modifies near-infrared band gaps in fluorescent single-walled carbon nanotubes. *Science* **2010**, *330*, 1656–1659.

17. Piao, Y. M.; Meany, B.; Powell, L. R.; Valley, N.; Kwon, H.; Schatz, G. C.; Wang, Y. H. Brightening of carbon nanotube photoluminescence through the incorporation of sp^3 defects. *Nat. Chem.* **2013**, *5*, 840–845.
18. Miyauchi, Y.; Iwamura, M.; Mouri, S.; Kawazoe, T.; Ohtsu, M.; Matsuda, K. Brightening of excitons in carbon nanotubes on dimensionality modification. *Nat. Photon.* **2013**, *7*, 715–719.
19. Santos, S. M.; Yuma, B.; Berciaud, S.; Shaver, J.; Gallart, M.; Gilliot, P.; Cognet, L.; Lounis, B. All-optical trion generation in single-walled carbon nanotubes. *Phys. Rev. Lett.* **2011**, *107*, 187401.
20. Matsunaga, R.; Matsuda, K.; Kanemitsu, Y. Observation of charged excitons in hole-doped carbon nanotubes using photoluminescence and absorption spectroscopy. *Phys. Rev. Lett.* **2011**, *106*, 037404.
21. Park, J. S.; Hirana, Y.; Mouri, S.; Miyauchi, Y.; Nakashima, N.; Matsuda, K. Observation of negative and positive trions in the electrochemically carrier-doped single-walled carbon nanotubes. *J. Am. Chem. Soc.* **2012**, *134*, 14461–14466.
22. Ma, X.; Adamska, L.; Yamaguchi, H.; Yalcin, S. E.; Tretiak, S.; Doorn, S. K.; Htoon, H. Electronic structure and chemical nature of oxygen dopant states in carbon nanotubes. *ACS Nano* **2014**, *8*, 10782–10789.
23. Hartmann, N. F.; Yalcin, S. E.; Adamska, L.; Hároz, E. H.; Ma, X.; Tretiak, S.; Htoon, H.; Doorn, S. K. Photoluminescence imaging of solitary dopant sites in covalently doped single-wall carbon nanotubes. *Nanoscale* **2015**, *7*, 20521–20530.
24. Hartmann, N. F.; Velizhanin, K. A.; Haroz, E. H.; Kim, M.; Ma, X.; Wang, Y.; Htoon, H.; Doorn, S. K. Photoluminescence dynamics of aryl sp3 defect states in single-walled carbon nanotubes. *ACS Nano* **2016**, *10*, 8355–8365.
25. Ma, X.; Baldwin, J. K.; Hartmann, N. F.; Doorn, S. K.; Htoon, H. Solid-state approach for fabrication of photostable, oxygen-doped carbon nanotubes. *Adv. Funct. Mater.* **2015**, *25*, 6157–6164.
26. Chen, J.; Dhall, R.; Hou, B.; Yang, S.; Wang, B.; Kang, D.; Cronin, S. B. Enhanced photoluminescence in air-suspended carbon nanotubes by oxygen doping. *Appl. Phys. Lett.* **2016**, *109*, 153109.
27. Chiu, C. F.; Saidi, W. A.; Kagan, V. E.; Star, A. Defect-induced near-infrared photoluminescence of single-walled carbon nanotubes treated with polyunsaturated fatty acids. *J. Am. Chem. Soc.* **2017**, *139*, 4859–4865.
28. Wei, X.; Tanaka, T.; Akizuki, N.; Miyauchi, Y.; Matsuda, K.; Ohfuchi, M.; Kataura, H. Single-chirality separation and optical properties of (5,4) single-wall carbon nanotubes. *J. Phys. Chem. C* **2016**, *120*, 10705–10710.
29. Kilina, S.; Ramirez, J.; Tretiak, S. Brightening of the lowest exciton in carbon nanotubes *via* chemical functionalization. *Nano Lett.* **2012**, *12*, 2306–2312.
30. Ramirez, J.; Mayo, M. L.; Kilina, S.; Tretiak, S. Electronic structure and optical spectra of semiconducting carbon nanotubes functionalized by diazonium salts. *Chem. Phys.* **2013**, *413*, 89–101.

31. Strano, M. S.; Dyke, C. A.; Usrey, M. L.; Barone, P. W.; Allen, M. J.; Shan, H.; Kittrell, C.; Hauge, R. H.; Tour, J. M.; Smalley, R. E. Electronic structure control of single-walled carbon nanotube functionalization. *Science* **2003**, *301*, 1519–1522.
32. Shiraki, T.; Shiraishi, T.; Juhász, G.; Nakashima, N. Emergence of new red-shifted carbon nanotube photoluminescence based on proximal doped-site design. *Sci. Rep.* **2016**, *6*, 28393.
33. Maeda, Y.; Kato, T.; Hasegawa, T.; Kako, M.; Akasaka, T.; Lu, J.; Nagase, S. Two-step alkylation of single-walled carbon nanotubes: Substituent effect on sidewall functionalization. *Org. Lett.* **2010**, *12*, 996–999.
34. Deng, S.; Zhang, Y.; Brozena, A. H.; Mayes, M. L.; Banerjee, P.; Chiou, W.-A.; Rubloff, G. W.; Schatz, G. C.; Wang, Y. Confined propagation of covalent chemical reactions on single-walled carbon nanotubes. *Nat. Comm.* **2011**, *2*, 382.
35. Maeda, Y.; Saito, K.; Akamatsu, N.; Chiba, Y.; Ohno, S.; Okui, Y.; Yamada, M.; Hasegawa, T.; Kako, M.; Akasaka, T. Analysis of functionalization degree of single-walled carbon nanotubes having various substituents *J. Am. Chem. Soc.* **2012**, *134*, 18101–18108.
36. Zhang, Y.; Valley, N.; Brozena, A.; Piao, Y. M.; Song, X.; Schatz, G. C.; Wang, Y. Propagative sidewall alkylcarboxylation induces red-shifted photoluminescence in single-walled carbon nanotubes. *J. Phys. Chem. Lett.* **2013**, *4*, 826–830.
37. Maeda, T.; Takehana, Y.; Yamada, M.; Suzuki, M.; Murakami, T. Control of the photoluminescence properties of single-walled carbon nanotubes by alkylation and subsequent thermal treatment. *Chem. Comm.* **2015**, *51*, 13462–13465.
38. Kwon, H.; Furmanchuk, A. O.; Kim, M.; Meany, B.; Guo, Y.; Schatz, G. C.; Wang, Y. Molecularly tunable fluorescent quantum defects. *J. Am. Chem. Soc.* **2016**, *138*, 6878–6885.
39. Maeda, Y.; Minami, S.; Takehana, Y.; Dang, J.-S.; Aota, S.; Matsuda, K.; Miyauchi, Y.; Yamada, M.; Suzuki, M.; Zhao, R.-S. Tuning of the photoluminescence and up-conversion photoluminescence properties of single-walled carbon nanotubes by chemical functionalization. *Nanoscale* **2016**, *8*, 16916–16921.
40. Brozena, A. H.; Leeds, J. D.; Zhang, Y.; Fourkas, J. T.; Wang, Y. Controlled defects in semiconducting carbon nanotubes promote efficient generation and luminescence of trions. *ACS Nano* **2014**, *8*, 4239–4247.
41. Powell, L. R.; Piao, Y.; Wang, Y. Optical excitation of carbon nanotubes drives localized diazonium reactions. *J. Phys Chem. Lett.* **2016**, *7*, 3690–3694.
42. He, X.; Hartmann, N. F.; Ma, X.; Kim, Y.; Ihly, R.; Blackburn, J. L.; Gao, W.; Kono, J.; Yomogida, Y.; Hirano, A.; Tanaka, T.; Kataura, H.; Htoon, H.; Doorn, S. K. Tunable room-temperature single-photon emission at telecom wavelengths from sp^3 defects in carbon nanotubes. *Nat. Photon.* **2017**, *11*, 577–582.

43. Powell, L. R.; Kim, M.; Wang, Y. Chirality-selective functionalization of semiconducting carbon nanotubes with a reactivity-switchable molecule. *J. Am. Chem. Soc.* **2017**, *139*, 12533–12540.
44. He, X.; Gifford, B. J.; Hartmann, N. F.; Ihly, R.; Ma, X.; Kilina, S. V.; Luo, Y; Shayan, K.; Strauf, S.; Blackburn, J. L.; Tretiak, S.; Doorn, S. K.; Htoon, H. Low-temperature single carbon nanotube spectroscopy of sp^3 quantum defects. *ACS Nano* **2017**, 11, 10785–10796.
45. Spataru, C. D.; Ismail-Beigi, S.; Benedict, L. X.; Louie, S. G. Excitonic effects and optical spectra of single-walled carbon nanotubes. *Phys. Rev. Lett.* **2004**, *92*, 077402.
46. Chang, E.; Bussi, G.; Ruini, A.; Molinari, E. Excitons in carbon nanotubes: An *ab initio* symmetry-based approach. *Phys. Rev. Lett.* **2004**, *92*, 196401.
47. Perebeinos, V.; Tersoff, J.; Avouris, P. Mobility in carbon nanotubes at finite carrier density. *Nano Lett.* **2006**, *6*, 205–208.
48. Zhao, H. B.; Mazumdar, S. Electron-electron interaction effects on the optical excitations of semiconducting single-walled carbon nanotubes. *Phys. Rev. Lett.* **2004**, *93*, 157402.
49. Tretiak, S.; Kilina, S.; Piryatinski, A.; Saxena, A.; Martin, R. L.; Bishop, A. R. Excitons and peierls distortion in conjugated carbon nanotubes. *Nano Lett.* **2007**, *7*, 86–92.
50. Kilina, S.; Tretiak, S. Excitonic and vibrational properties of single-walled semiconducting carbon nanotubes. *Adv. Funct. Mater.* **2007**, *17*, 3405–3420.
51. Kilina, S.; Kilin, D.; Tretiak, S. Light-driven and phonon-assisted dynamics in organic and semiconducting nanostructures. *Chem. Rev.* **2015**, *115*, 5929–5978.
52. Gifford, B. J.; Kilina, S.; Htoon, H.; Doorn, S. K.; Tretiak, S. Exciton localization and optical emission in aryl-functionalized carbon nanotubes. *J. Phys. Chem. C* **2018**, *122*, 1828–1838.
53. Shreve, A. P.; Haroz, E. H.; Bachilo, S. M.; Weisman, R. B.; Tretiak, S.; Kilina, S.; Doorn, S. K. Determination of exciton-phonon coupling elements in single walled carbon nanotubes via raman overtone analysis. *Phys. Rev. Lett.* **2007**, *98*, 037405.
54. Kim, M.; Adamska, L.; Hartmann, N. F.; Kwon, H.; Liu, J.; Velizhanin, K. A.; Piao, Y.; Powell, L. R.; Meany, B.; Doorn, S. K.; Tretiak, S.; Wang, Y. Fluorescent carbon nanotube defects manifest substantial vibronic reorganization. *J. Phys. Chem. C* **2016,** *120*, 11268–11276.
55. Ardizzone, V.; Chassagneux, Y.; Vialla, F.; Delport, G.; Delcamp, C.; Belabas, N.; Deleporte, E.; Roussignol, Ph.; Robert-Philip, I.; Voisin, C.; Lauret, J. S. Strong reduction of exciton-phonon coupling in single-wall carbon nanotubes of high crystalline quality: Insight into broadening mechanisms and exciton localization. *Phys. Rev. B* **2015**, *91*, 121410(R).
56. Galland, C.; Högele, A.; Türeci, H. E.; Imamoğlu, A. Non-markovian decoherence of localized nanotube excitons by acoustic phonons. *Phys. Rev. Lett.* **2008**, *101*, 067402.

57. Sarpkaya, I.; Ahmadi, E. D.; Shepard, G. D.; Mistry, K. S.; Blackburn, J. L.; Strauf, S. Strong acoustic phonon localization in copolymer-wrapped carbon nanotubes. *ACS Nano* **2015**, *9*, 6383–6393.
58. Vialla, F.; Chassagneux, Y.; Ferreira, R.; Roquelet, C.; Diederichs, C.; Cassabois, G.; Roussignol, P.; Lauret, J.-S.; Voisin, C. Unifying the low-temperature photoluminescence spectra of carbon nanotubes: The role of acoustic phonon confinement. *Phys. Rev. Lett.* **2014**, *113*, 057402.
59. Aharonovich, I.; Englund, D.; Toth, M. Solid-state single-photon emitters. *Nat. Photon.* **2016**, *10*, 631–641.
60. Buckley, S.; Rivoire, K.; Vuckovic, J. Engineered quantum dot single photon sources. *Rep. Prog. Phys.* **2012**, *75*, 126503.
61. Perebeinos, V. Two dimensions and one photon. *Nat. Nanotechnol.* **2015**, *10*, 485–486.
62. Iwamura, M.; Akizuki, N.; Miyauchi, Y.; Mouri, S.; Shaver, J.; Gao, Z.; Cognet, L.; Lounis, B.; Matsuda, K. Nonlinear photoluminescence spectroscopy of carbon nanotubes with localized exciton states. *ACS Nano* **2014**, *8*, 11254–11260.
63. Berciaud, S.; Cognet, L.; Lounis, B. Luminescence decay and the absorption cross section of individual single-walled carbon nanotubes. *Phys. Rev. Lett.* **2008**, *101*, 077402.
64. Harutyunyan, H.; Gokus, T.; Green, A. A.; Hersam, M. C.; Allegrini, M.; Hartschuh, A. Defect-induced photoluminescence from dark excitonic states in individual single-walled carbon nanotubes. *Nano Lett.* **2009**, *9*, 2010–2014.
65. Gokus, T.; Cognet, L.; Duque, J. G.; Pasquali, M.; Hartschuh, A.; Lounis, B. Mono- and biexponential luminescence decays of individual single-walled carbon nanotubes. *J. Phys. Chem. C* **2010**, *114*, 14025–14028.
66. Matsunaga, R.; Miyauchi, Y.; Matsuda, K.; Kanemitsu, Y. Symmetry-induced nonequilibrium distributions of bright and dark exciton states in single carbon nanotubes. *Phys. Rev. B* **2009**, *80*, 115436.
67. Perebeinos, V.; Avouris, P. Phonon and electronic nonradiative decay mechanisms of excitons in carbon nanotubes. *Phys. Rev. Lett.* **2008**, *101*, 057401.
68. Lin, C.-W.; Weisman, R. B. *In vivo* detection of single walled carbon nanotubes: Progress and challenges. *Nanomed.* **2016**, *11*, 2885–2888.
69. Akizuki, N.; Aota, S.; Mouri, S.; Matsuda, K.; Miyauchi, Y. Efficient near-infrared up-conversion photoluminescence in carbon nanotubes. *Nat. Comm.* **2015**, *6*, 8920.
70. Aota, S.; Akizuki, N.; Mouri, S.; Matsuda, K.; Miyauchi, Y. Upconversion photoluminescence imaging and spectroscopy of individual single-wall carbon nanotubes. *Appl. Phys. Exp.* **2016**, *9*, 045103.
71. Kwon, H.; Kim, M.; Meany, B.; Piao, Y.; Powell, L. R.; Wang, Y. Optical probing of local pH and temperature in complex fluids with covalently functionalized semiconducting carbon nanotubes. *J. Phys. Chem. C* **2015**, *119*, 3733–3739.

72. Shiraki, T.; Onitsuka, H.; Shiraishi, T.; Nakashima, N. Near infrared photoluminescence modulation of single-walled carbon nanotubes based on a molecular recognition approach. *Chem. Comm.* **2016**, *52*, 12972–12975.
73. Lounis, B.; Orrit, M. Single-photon sources. *Rep. Prog. Phys.* **2005**, *68* 1129–1179.
74. Aharonovich, I.; Castelletto, S.; Simpson, D. A.; Su, C.-H.; Greentree, A. D.; Prawer, S. Diamond-based single-photon emitters. *Rep. Prog. Phys.* **2011**, *74* 076501.
75. Gordon, L.; Weber, J. R.; Varley, J. B.; Janotti, A.; Awschalom, D. D.; Van de Walle, C. G. Quantum computing with defects. *MRS Bull.* **2013**, *38*, 802–807.
76. Miyazawa, T.; Takemoto, K.; Nambu, Y.; Miki, S.; Yamashita, T.; Terai, H.; Fujiwara, M.; Sasaki, M.; Sakuma, Y.; Takatsu, M.; Yamamoto, T.; Arakawa, Y. Single-photon emission at 1.5 μm from an InAs/InP quantum dot with highly suppressed multi-photon emission probabilities. *Appl. Phys. Lett.* **2016**, *109*, 132106.
77. Tran, T. T.; Bray, K.; Ford, M. J.; Toth, M.; Aharonovich, I. Quantum emission from hexagonal boron nitride monolayers. *Nat. Nanotechnol.* **2016**, *11*, 37–41.
78. Bachilo, S. M.; Strano, M. S.; Kittrell, C.; Hauge, R. H.; Smalley, R. E.; Weisman, R. B. Structure-assigned optical spectra of single-walled carbon nanotubes. *Science* **2002**, *298*, 2361–2366.
79. Htoon, H.; O'Connell, M. J.; Cox, P. J.; Doorn, S. K.; Klimov, V. I. Low temperature emission spectra of individual single-walled carbon nanotubes: Multiplicity of subspecies within "single species" nanotube ensembles. *Phys. Rev. Lett.* **2004**, *93*, 027401.
80. Georgi; C.; Green, A. A.; Hersam, M. C.; Hartschuh, A. Probing exciton localization in single-walled carbon nanotubes using high-resolution near-field microscopy. *ACS Nano* **2010**, *4*, 5914–5920.
81. Hofmann, M. S.; Noe, J.; Kneer, A.; Crochet, J. J.; Hogele, A. Ubiquity of exciton localization in cryogenic carbon nanotubes. *Nano Lett.* **2016**, *16*, 2958–2962.
82. Hoegele, A.; Galland, C.; Winger, M.; Imamoglu, A. Photon antibunching in the photoluminescence spectra of a single carbon nanotube. *Phys. Rev. Lett.* **2008**, *100*, 217401.
83. Hofmann, M. S.; Gluckert, J. T.; Noe, J.; Bourjau, C.; Dehmel, R.; Hoegele, A. Bright, Long-lived and coherent excitons in carbon nanotube quantum dots. *Nat. Nanotech.* **2013**, *8*, 502–505.
84. Ma, X.; Roslyak, O.; Duque, J. G.; Doorn, S. K.; Piryatinski, A.; Dunlap, D. H.; Htoon, H. Influences of exciton diffusion and exciton-exciton annihilation on photon emission statistics of carbon nanotubes. *Phys. Rev. Lett.* **2015**, *115*, 017401.
85. Endo, T.; Ishi-Hayase, J.; Maki, H. Photon antibunching in single-walled carbon nanotubes at telecommunication wavelengths and room temperature. *Appl. Phys. Lett.* **2015**, *106*, 113106.

86. Ishii, A.; Uda, T.; Kato, Y. K. Room-temperature single photon emission from micron-long air-suspended carbon nanotubes. *Phys. Rev. Appl.* **2017**, *8*, 054039.
87. Ma, X.; Hartmann, N. F.; Baldwin, J. K. S.; Doorn, S. K.; Htoon, H. Room-temperature single-photon generation from solitary dopants of carbon nanotubes. *Nat. Nanotechnol.* **2015**, *10*, 671–675.
88. Sarpkaya, I.; Walden-Newman, W.; Wang, X. S.; Hone, J.; Wong, C. W.; Strauf, S. Prolonged spontaneous emission and dephasing of localized excitons in air-bridged carbon nanotubes. *Nat. Comm.* **2013**, *4*, 2152.
89. Flagg, E.; Muller, A.; Robertson, J. W.; Founta, S.; Deppe, D. G.; Xiao, M.; Salamo, G. J.; Shih, C. K. Resonantly driven coherent oscillations in a solid-state quantum emitter. *Nat. Phys.* **2009**, *5*, 203–207.
90. Ates, S.; Ulrich, S. M.; Reitzenstein, S.; Loffler, A.; Forchel, A.; Michler, P. Post-selected indistinguishable photons from the resonance fluorescence of a single quantum dot in a microcavity. *Phys. Rev. Lett.* **2009**, *103*, 167402.
91. Matthiesen, C.; Geller, M.; Schulte, C. H. H.; Le Gall, C.; Hansom, J.; Li, Z. Y.; Hugues, M.; Clarke, E.; Atature, M. Phase-locked indistinguishable photons with synthesized waveforms from a solid-state source. *Nat. Comm.* **2013**, *4*, 1600.
92. Ma, X.; Htoon, H. Tailoring the photophysical properties of carbon nanotubes by photonic nanostructures. *Mod. Phys. Lett. B* **2015**, *29*, 1530004.
93. Imamura, S.; Watahiki, R.; Miura, R.; Shimada, T.; Kato, Y. Optical control of individual carbon nanotube light emitters by spectral double resonance in silicon microdisk resonators. *Appl. Phys. Lett.* **2013**, *102*, 161102.
94. Miura, R.; Imamura, S.; Ohta, R.; Ishii, A.; Liu, X.; Shimada, T.; Iwamoto, S.; Arakawa, Y.; Kato, Y. Ultralow mode volume photonic crystal nanobeam cavities for high-efficiency coupling to individual carbon nanotube emitters. *Nat. Comm.* **2014**, *5*, 5580.
95. Watahiki, R.; Shimada, T.; Zhao, P.; Chiashi, S.; Iwmoto, S.; Arakawa, Y.; Maruyama, S.; Kato, Y. Kato. Enhancement of carbon nanotube photoluminescence by photonic crystal nanocavities. *Appl. Phys. Lett.* **2012**, *101*, 141124.
96. Jeantet, A.; Chassagneux, Y.; Raynaud, C.; Roussignol, Ph.; Lauret, J. S.; Besga, B.; Esteve, J.; Reichel, J.; Voisin, C. Widely tunable single-photon source from a carbon nanotube in the purcell regime. *Phys. Rev. Lett.* **2016**, *116*, 247402.
97. Jeantet, A.; Chassagneux, Y.; Claude, T.; Roussignol, P.; Lauret, J. S.; Reichel, J.; Voisin, C. Exploiting one-dimensional exciton-phonon coupling for tunable and efficient single-photon generation with a carbon nanotube. *Nano Lett.* **2017**, *17*, 4184–4188.
98. Koenderink, A. F. Single-photon nanoantennas. *ACS Photonics* **2017**, *4*, 710–722.
99. Ma, X.; Roslyak, O.; Wang, F.; Duque, J. G.; Piryatinski, A.; Doorn, S. K.; Htoon, H. Influence of exciton dimensionality on spectral diffusion of single-walled carbon nanotubes. *ACS Nano* **2014**, *8*, 10613–10620.

100. Luo, Y.; Ahmadi, E. D.; Shayan, K.; Ma, Y.; Mistry, K. S.; Zhang, C.; Hone, J.; Blackburn, J. L.; Strauf, S. Purcell-enhanced quantum yield from carbon nanotube excitons coupled to plasmonic nanocavities. *Nat. Comm.* **2017**, *8*, 1413.
101. Zakharko, Y.; Graf, A.; Zaumseil, J. Plasmonic crystals for strong light-matter coupling in carbon nanotubes. *Nano Lett.* **2016**, *16*, 6504–6510.
102. Graf, A.; Tropf, L.; Zakharko, Y.; Zaumseil, J.; Gather, M. C. Near-infrared exciton-polaritons in strongly coupled single-walled carbon nanotube microcavities. *Nat. Comm.* **2016**, *7*, 13078.
103. Zakharko, Y.; Graf, A.; Schiesl, S. P.; Hahnlein, B.; Pezoldt, J.; Gather, M. C.; Zumseil, J. Broadband tunable polarization-selective and directional emission of (6,5) carbon nanotubes coupled to plasmonic crystals. *Nano Lett.* **2016**, *16*, 3278–3284.
104. Shayan, K.; Rabut, C.; Kong, X.; Li, X.; Luo, Y.; Mistry, K. S.; Blackburn, J. L.; Lee, S. S.; Strauf, S. Broadband light collection efficiency enhancement of carbon nanotube excitons coupled to metallo-dielectric antenna arrays. *ACS Photonics* **2018**, *5*, 289–294.
105. Staude, I.; Khardikov, V. V.; Fofang, N. T.; Liu, S.; Decker, M.; Neshev, D. N.; Luk, T. S.; Brener, I.; Kivshar, Y. S. Shaping photoluminescence spectra with magnetoelectric resonances in all-dielectric nanoparticles. *ACS Photonics* **2015**, *2*, 172–177.
106. Ma, X.; James, A. R.; Hartmann, N. F.; Baldwin, J. K.; Dominguez, J.; Sinclair, M. B.; Luk, T. S.; Wolf, O.; Liu, S.; Doorn, S. K.; Htoon, H.; Brener, I. Solitary oxygen dopant emission from carbon nanotubes modified by dielectric metasurfaces. *ACS Nano* **2017**, *11*, 6431–6439.
107. Misewich, J.; Martel, R.; Avouris, P.; Tsang, J.; Heinze, S.; Tersoff, J. Electrically induced optical emission from a carbon nanotube FET. *Science* **2003**, *300*, 783–786.
108. Marty, L.; Adam, E.; Albert, L.; Doyon, R; Menard, D.; Martel, R. Exciton formation and annihilation during 1D impact excitation of carbon nanotubes. *Phys. Rev. Lett.* **2006**, *96*, 136803.
109. Jakubka, F.; Backes, C.; Gannott, F.; Mundloch, U.; Hauke, F.; Hirsch, A.; Zaumseil, J. Mapping charge transport by electroluminescence in chirality-selected carbon nanotube networks. *ACS Nano* **2013**, *7*, 7428–7435.
110. Mori, T.; Yamauchi, Y.; Honda, S.; Maki, H. An electrically driven ultrahigh-speed on-chip light emitter based on carbon nanotubes. *Nano Lett.* **2014**, *14*, 3277–3283.
111. Khasminskaya, S.; Pyatkov, F.; Flavel, B. S.; Pernice, W. H. P.; Krupke, R. Waveguide-integrated light-emitting carbon nanotubes. *Adv. Mater.* **2014**, *26*, 3465–3472.
112. Pyatkov, F.; Futterling, V.; Khasminskaya, S.; Flavel, B. S.; Hennrich, F.; Kappes, M. M.; Krupke, R.; Pernice, W. H. P. Cavity-enhanced light emission from electrically driven carbon nanotubes. *Nat. Photon.* **2016**, *10*, 420–427.

113. Khasminskaya, S.; Pyatkov, F.; Slowik, K.; Ferrari, S.; Kahl, O.; Kovalyuk, V.; Rath, P.; Vetter, A.; Hennrich, F.; Kappes, M. M.; Gol'tsman, G.; Korneev, A.; Rockstuhl, C.; Krupke, R.; Pernice, W. H. P. Fully integrated quantum photonic circuit with an electrically driven light source. *Nat. Photon.* **2016**, *10*, 727–732.
114. Graf, A.; Held, M.; Zakharko, Y.; Tropf, L.; Gather, M. C.; Zaumseil, J. Electrical pumping and tuning of exciton-polaritons in carbon nanotube microcavities. *Nat. Mater.* **2017**, *16*, 911–917.